Elevated protein lactylation promotes immunosuppressive microenvironment and therapeutic resistance in pancreatic ductal adenocarcinoma

Kang Sun[1,2,3,4,#], Xiaozhen Zhang[1,2,3,4,#],Jiatao Shi[1,2,3,4,#], Jinyan Huang[1,2,3,4,#], Sicheng Wang[1,2,3,4], Xiang Li[1,2,3,4], Haixiang Lin[1,2,3,4], Danyang Zhao[1,2,3,4], Mao Ye[1,2,3,4], Sirui Zhang[1,2,3,4],Li Qiu[1,2,3,4], Minqi Yang[1,2,3,4], Chuyang Liao[1,2,3,4], Lihong He[1,2,3,4], Mengyi Lao[1,2,3,4], Jinyuan Song[1,2,3,4], Na Lu[1,2,3,4], Yongtao Ji[1,2,3,4], Hanshen Yang[1,2,3,4], Linyue Liu[1,2,3,4], Xinyuan Liu[1,2,3,4], Yan Chen[1,2,3,4], Shicheng Yao[1,2,3,4], Qianhe Xu[1,2,3,4], Jieru Lin[1,2,3,4], Yan Mao[1,2,3,4], Jingxing Zhou[1,2,3,4], Xiao Zhi[1,2,3,4], Ke Sun[1,2,3,4], Xiongbin Lu[1,2,3,4,*], Xueli Bai[1,2,3,4,5,*], Tingbo Liang[1,2,3,4,5,*]

1. Department of Hepatobiliary and Pancreatic Surgery, the First Affiliated Hospital, School of Medicine, Zhejiang University, Hangzhou, Zhejiang, China.

2. Zhejiang Provincial Key Laboratory of Pancreatic Disease, the First Affiliated Hospital, School of Medicine, Zhejiang University, Hangzhou, Zhejiang, China.

3. MOE Joint International Research Laboratory of Pancreatic Diseases, Hangzhou, China.

4. Zhejiang Provincial Clinical Research Center for the Study of Hepatobiliary & Pancreatic Diseases, Zhejiang University, Hangzhou, China.

5. Cancer Center, Zhejiang University, Hangzhou, China.

# These authors contributed equally.

*Corresponding authors:

Address correspondence to Tingbo Liang: Teaching and Research Center of the First College of Zhejiang University, No. 17, Laozheda Straight Road, Xiaoying Street, Shangcheng District, Hangzhou, Zhejiang Province, China. Phone: +86-0571-87236601. E-mail: liangtingbo@zju.edu.cn.

Address correspondence to Xueli Bai: Teaching and Research Center of the First College of Zhejiang University, No. 17, Laozheda Straight Road, Xiaoying Street, Shangcheng District, Hangzhou, Zhejiang Province, China. Phone: +86-0571-87236857. E-mail: shirleybai@zju.edu.cn

Address correspondence to Xiongbin Lu: Teaching and Research Center of the First College of Zhejiang University, No. 17, Laozheda Straight Road, Xiaoying Street, Shangcheng District, Hangzhou, Zhejiang Province, China. Phone: +86-0571-87236058, E-mail: xiongbinlu@zju.edu.cn.

Key words: Pancreatic ductal adenocarcinoma, lactylation, glycolysis, immune checkpoint blockade therapy, immunosuppressive tumor microenvironment, endosulfine alpha

Declaration of interests

The authors declare that they have no competing interests.

Abstract

Metabolic reprogramming shapes tumor microenvironment (TME) and may lead to immunotherapy resistance in pancreatic ductal adenocarcinoma (PDAC). Elucidating the impact of pancreatic cancer cell metabolism in the TME is essential to therapeutic interventions. “Immune cold” PDAC is characterized by elevated lactate levels resulting from tumor cell metabolism, abundance of pro-tumor macrophages, and reduced cytotoxic T cell in the TME. Analysis of ^{18}F-FDG uptake in patients showed that increased global protein lactylation in PDAC correlates with worse clinical outcomes in immunotherapy. Inhibition of lactate production in pancreatic tumors via glycolysis or mutant-KRAS inhibition reshaped the TME, thereby increasing their sensitivity to immune checkpoint blockade (ICB) therapy. In pancreatic tumor cells, lactate induces K63 lactylation of Endosulfine alpha (ENSA-K63la), a crucial step that triggers STAT3-CCL2 signaling. Consequently, elevated CCL2 secreted by tumor cells facilitates tumor-associated macrophage (TAM) recruitment to the TME. High levels of lactate also drive transcriptional reprogramming in TAMs via ENSA-STAT3 signaling, promoting an immunosuppressive environment. Targeting ENSA-K63la or CCL2 enhances the efficacy of ICB therapy in murine and humanized pancreatic tumor models. In conclusion**,** elevated lactylation reshapes the TME and promotes immunotherapy resistance in PDAC. Therapeutic approach targeting ENSA-K63la or CCL2 has shown promise in sensitizing pancreatic cancer immunotherapy.

Introduction

Pancreatic cancer remains a significant challenge in clinical practice, with 5-year survival rates very low at approximately 12% (1). Immunotherapy is considered promising for enabling long-term survival or recovery(2). However, in a randomized controlled trial (RCT) conducted at our center, while the combination use of immune checkpoint blockage (ICB) can improve the overall response rate, no clear survival benefit was observed and the benefit of adding PD-1 antibody sintilimab for advanced pancreatic cancer was not supported (3). A significant portion of pancreatic cancer patients are resistant to immunotherapy.

During tumor initiation and progression, interactions between tumor cells, immunocytes and stromal cells within the tumor microenvironment (TME) mutually influence each other. This dynamic interplay triggers a series of molecular biological changes that modify tumor metabolism and the microenvironment, culminating in the formation of a complex tumor ecosystem. This ecosystem collectively dictates the treatment sensitivity (4). Tumor cells undergo metabolic reprogramming to gain growth advantages (5). driven by genetic mutations and environmental constraints (6, 7). Key somatic mutations such as KRAS, TP53, CDKN2A, and SMAD4 are prevalent in pancreatic cancer and significantly impact metabolic processes (8, 9). Furthermore, pancreatic cancer progression is marked by vascular insufficiency, nutrient deficiency, hypoxia, and extracellular matrix alterations, which further contribute to metabolic shifts (10).

Consequently, the metabolic profile of pancreatic cancer exhibits unique complexity and diversity compared to other malignancies, resulting in distinctive metabolic dependencies. Moreover, the heterogeneous genomic and environmental landscapes of pancreatic cancers contribute to tissue heterogeneity, leading to differential responses to therapeutic interventions. Therefore, a comprehensive exploration of the tissue, immune, metabolic, and molecular characteristics underlying resistance to immunotherapy in pancreatic cancer is essential. Identifying the pivotal drivers of resistance can facilitate precise interventions and enable the identification of patient subpopulations likely to benefit from immunotherapy, thereby enhancing treatment outcomes.

Pancreatic cancer is recognized for its high resistance to immune interventions, with a significant portion of patients classified as immune exclusive or immune desert (2, 11). This poor immune profile often manifests with myeloid cell accumulation and sparse T cell presence, contributing to resistance against immunotherapies (12-14). Metabolic reprogramming plays a pivotal role in reshaping the immune microenvironment and is implicated in immunotherapy resistance (15). Analysis of data from TCGA-PAAD and GEO databases revealed that "immune cold" pancreatic ductal adenocarcinoma (PDAC) is characterized by heightened glycolytic activity, which correlates positively with pro-tumor macrophage infiltration and negatively with cytotoxic T cell infiltration. Clinically, patients exhibiting low ^{18}F-FDG uptake demonstrated improved responses to immunochemotherapy and prolonged progression-free survival (PFS). These findings

underscore the impact of elevated glycolysis on immunotherapy resistance and underscore the need for identifying effective treatment modalities.

Lactate, as the end product of glycolysis, exerts significant influence on the immune microenvironment (16). Studies indicate that elevated lactate levels can impair the migration and cytotoxic function of $CD8^+$ T cells, while promoting polarization of macrophages towards a pro-tumor phenotype and inhibiting monocyte differentiation into dendritic cells (DCs). However, these observations are largely derived from in vitro investigations, and the precise role of lactate as a signaling molecule within the in vivo microenvironment remains ambiguous (17-19). Crucially, these studies have not accounted for spatial gradients in lactate distribution, spatial variations in immune cell infiltration, and the heterogeneous responses of immune cells to lactate. Therefore, further in vivo experiments are essential to elucidate how lactate remodels the immune microenvironment. Recent research has identified lactate as a versatile signaling molecule (2). Zhao et al. demonstrated that lysine lactylation contributes to epigenetic regulation (20). Lactylation has been implicated in regulating tissue homeostasis, metabolic transitions, tumor progression, and resistance to chemotherapy (20-23). Previous studies on lactylation have predominantly focused on histone lactylation. Yet, similar to other acylation modifications, targeting histone lactylation may lead to unintended off-target effects (23, 24). Therefore, we are interested in non-histone lactylation to identify critical proteins and specific lactylation sites for potential therapeutic

intervention. In this study, we found that glycolysis-dependent ENSA-K63 lactylation inactivated PP2A, thereby sustaining SRC-S12 phosphorylation and STAT3-Y705 phosphorylation. Activation of STAT3 is known to enhance macrophage chemotaxis and promote pro-tumor phenotypes. To counteract this pathway, we utilized a cell-penetrating peptide specific to ENSA-K63 lactylation, effectively blocking K63 lactylation and consequently inhibiting STAT3 activation in both tumor cells and macrophages. This strategy has shown promise in sensitizing immunotherapy approaches for pancreatic cancer.

Results

Elevated lactylation is correlated with immunosuppressive TME in PDAC

As a metabolic waste and an end product from glycolysis, lactate was known to be associated with muscle fatigue and potential tissue harm (25). However, recent studies have unveiled a novel function of lactate: it can modify lysine residues on proteins, known as lysine lactylation (Kla or Klac). Recent studies have shown that lactylation promotes glycolysis in a feedback loop, sustaining the nuclear NAD+ salvage pathway, thereby driving oncogenesis and metastasis(26-28). However, the regulation of the immune microenvironment by lactylation in PDAC remains poorly understood. Using multiplex immunohistochemistry (mIHC), we observed that pan-lysine lactylation (Pan-Kla) levels were dramatically elevated in pancreatic tumor tissues compared to their paired para-cancerous normal tissues (**Figure 1, A and B**). Increased levels of Pan-Kla modification indicated anaerobic glycolysis-related lactate accumulation in the tumor tissues. In the glycolysis pathway, SLC2A1 serves as the primary glucose transporter. Hexokinase 2 (HK2) acts as the rate-limiting enzyme responsible for converting glucose to glucose-6-phosphate, which is the first crucial step in this pathway. LDHA plays a pivotal role in converting pyruvate into lactate, while SLC16A3 functions as the transporter responsible for moving lactate into the tumor microenvironment (20, 29). We found that these key genes are all upregulated in the PDAC, and as expected, their expression levels are correlated well with Pan-Kla levels (**Figure 1C and Supplementary Figure 1A**). Pan-Kla level analysis using tissue microarrays

demonstrated that elevated levels of Pan-Kla were correlated with worse overall survival (**Figure 1D**).

To study the impact of protein lactylation on the tumor immune microenvironment, we applied a 24-color high dimensional immunoprofiling panel in spectral flow cytometry (CyTek) to identify the tumor-infiltrated immune cells in fresh PDAC tissue samples. A total of 20 resected pancreatic tumor tissues were divided into two groups according to their global lactylation levels (**Supplementary Figure 1B and Supplementary Table 1**). The group with high Pan-Kla levels exhibited a higher level of macrophage ($CD11b^+HLADR^+CD68^+$) infiltration but lower level of infiltration for $CD8^+$ T ($CD3^+CD4^-CD8^+$) cells (**Figure 1E and Supplementary Figure 1C**). Next, we used mIHC staining assay to validate the impact of lactylation on the tumor immune profiles with resectable PDAC using tissue microarrays. Consistently, the "High Pan-Kla" group showed higher infiltration of monocytes/macrophages (CD14+ or CD68+) and lower infiltration of $CD8^+$ T cells (CD8+) in comparison with the “Low Pan-Kla” group (**Figure 1F**). Collectively, elevated lactylation was associated with a more immunosuppressive TME in PDAC, characterized by macrophage accumulation and limited $CD8^+$ T cell infiltration.

Lactate is produced by tumors and accumulates in the tumor microenvironment (TME) through SLC16A3. The concentration gradient of lactate influences the biological functions of cells near the tumor. Given that elevated lactylation impacts immune cell

infiltration, we hypothesized that heterogeneous spatial distribution and different responsiveness to lactate could further reshape immune cell function. Among different cell types in the TME of patients with PDAC, lactylation was highest in macrophages (**Figure 1G**). Lactylation was significantly elevated in tumor-associated macrophages (TAMs) compared to macrophages in peripheral blood, supporting the idea that tumor cell metabolism reprograms macrophages in the TME (**Figure 1G**). 2-NBDG, a glucose analog, was used to detect glucose uptake and utilization both in vivo or in vitro(30). Compared to peripheral blood, glucose utilization in TAMs was not elevated in tumor tissue and did not constitute the majority of glucose utilization among immune cells (**Figure 1G**). This demonstrated that the elevated lactylation levels in TAMs were not derived from increased glycolysis activity but likely from elevated lactate intake from the TME.

To further explore the impact of elevated lactate accumulation on infiltrated TAMs and $CD8^+$ T cells at the single-cell level, we analyzed public single-cell RNA sequencing (scRNA-seq) datasets of PDAC (GSE205013; CRA001160; PHS002371; GSE212966) (**Supplementary Figure 1D**)(31-34). Patient tumors were divided into two groups based on median glycolysis scores determined by the expression levels of glycolysis-related genes (SLC2A1, HK2, GPI1, PFKL, PGK, ALDOA, PGAM, GAPDH, PFKM, ENO1, PKM, LDHA, and SLC16A3) in tumor cells. Macrophages from tumors with high glycolysis scores underwent phenotype reprograming, presenting as changes of transcriptional

activity (such as NFKB1, STAT1, JUN and STAT3), elevating expression of pro-tumor inflammation markers and immune checkpoints (IL1A, IL1B, IL10, S100A8, S100A9, CCL2, CCL4, CD274, NT5E), and alongside decreasing expression of genes associated with $CD8^+$ T cell migration and activation (ICOS, CCL19, IFNG) (**Figure 1H and Supplementary Figure 1, E and F**). Correspondingly, $CD8^+$ T cells in tumors with high glycolysis scores exhibited a trend toward negative regulation of immune response and leukocyte activation. This is characterized by up-regulated expression of exhaustion markers (HAVCR2, CTLA4, TOX) and reduced expression of cytotoxicity and activation markers (GZMA, GZMK, TNF, LTB, CD69, TCF7, KLRB1) (**Figure 1I and Supplementary Figure 1F**). Together, these findings suggest that glycolysis and its associated lactylation contribute to an immunosuppressive TME, marked by enhanced accumulation of pro-tumor macrophages. Given their high level of lactylation, we reasoned that macrophages might play an important role in inhibiting T cell infiltration and function.

Elevated lactylation is associated with immunotherapy resistance in PDAC

Because of their association with immunosuppressive TME, we aimed to determine whether glycolysis and resultant lactylation contribute to immunotherapy resistance in PDAC. Flourine-18 fluorodeoxyglucose positron emission tomography/computed tomography (^{18}F-FDG PET/CT) has been widely used in clinic to reveal glucose metabolism abnormalities in infection and inflammation, yet its use in diagnosing primary

pancreatic cancer is uncommon (35). Our team previously performed a prospective cohort study that enrolled PDAC patients who received ^{18}F-FDG PET-CT scans before chemotherapy or immunochemotherapy between August 2021 and February 2023 (35). We reviewed this cohort and assessed whether the standard uptake value (SUV) on PET scans correlated with immunotherapy outcomes (**Supplementary Table 2**). Among the 51 patients, 26 received chemotherapy alone and 25 received immunochemotherapy plus chemotherapy. Based on median SUVmax (cutoff = 8.1), the cohort was divided into "High uptake" and "Low uptake" groups. The "Low uptake" group showed significantly improved progression-free survival (PFS) with immunochemotherapy compared to the "High uptake" group, although this effect was not observed with chemotherapy alone (**Figure 2A**). The overall response rate (ORR) was notably higher in the "Low uptake" group with immunochemotherapy (6/12) compared to the "High uptake" group (1/13). These findings suggest that elevated glycolysis may influence the response to immunochemotherapy in PDAC patients. Representative pre-treatment and post-treatment ^{18}F-FDG PET/CT images of patients who did or did not respond to immunochemotherapy are illustrated in **Figure 2B**.

To investigate the correlation between lysine lactylation levels in tumor tissues and clinical outcomes of PDAC patients, biopsy specimens from 31 patients enrolled in a randomized phase II CISPD3 trial (NCT03977272) were analyzed using immunohistochemical staining with Pan-Cytokeratin (Pan-CK) and Pan-Kla antibodies

(**Figure 2C and Supplementary Figure 2, A and B and Supplementary Table 3**). This trial evaluated whether combining Sintilimab (PD-1 monoclonal antibody) with modified FOLFIRINOX (mFFX) improves outcomes compared to mFFX alone for advanced pancreatic cancer (3). Elevated lactylation levels, measured by mean fluorescence intensity of Pan-Kla in tumor tissues, were significantly correlated with poorer patient survival (**Figure 2D**). Additionally, lactylation levels in tumor tissues demonstrated high specificity (86.7%), sensitivity (92.9%) and an Area Under the ROC Curve (AUC, 95.59) for predicting outcome of immunotherapy, using overall survival time as the outcome metric (**Figure 2E**). These findings collectively suggest that increased glycolysis and consequent protein lactylation in tumors are associated with immunotherapy resistance in PDAC, underscoring the potential utility of lactylation levels as predictive biomarkers in PDAC immunotherapy outcomes.

We further investigated whether pancreatic cancer tissue features contribute to immunotherapy resistance. Approximately 90% of pancreatic cancers harbor KRAS mutations. It has been long known that KRAS G12 mutations promote glycolysis and anabolic metabolism in cancer cells (36). Indeed, our analysis of the pancreatic cancer database in The Cancer Genome Atlas (TCGA-PAAD) revealed that tumors with KRAS G12 mutations had significantly higher glycolysis score than other tumors (**Figure 2F**). MRTX1133 is a newly synthesized selective KRAS-G12D inhibitor that entered clinical trials in 2023 (37, 38). Treatment of mouse KPC (*KrasG12D; Trp53R172H; Pdx1-Cre*)

cells with MTRX133 downregulated the expression of key genes in glycolysis, including SLC2A1, HK2, PFK, ENO1, LDHA, and SLC16A3 (**Figure 2G and Supplementary Figure 2C**). As a result, MRTX1133 significantly decreased the level of global lactylation in the tumor cells (**Figure 2G**). In the KPC cell-derived orthotopic mouse PDAC model, MRTX1133 treatment significantly decreased glucose utilization of the tumors shown by ^{18}F-FDG PET-CT **(Figure 2H)**, as well as inhibited tumor growth, but interestingly, the inhibition of KRAS dramatically sensitized the KPC tumors to anti-PD-1-based immune checkpoint blockade (**Figure 2I**). Analysis of tumor immune profiles with flow cytometry showed that treatment of MRTX1133 decreased tumor infiltration of bone-marrow-derived monocytes ($CD11b^+Ly6C^{high}$ $Ly6G^-$) and, particularly macrophages ($CD11b^+F4/80^+IA/IE^+$) and pro-tumoral macrophages ($ARG1^+$ macrophages) (**Figure 2J**). By contrast, MRTX1133 treatment increased $CD8^+$ T cell infiltration and activity (**Figure 2J**).

Inhibiting glycolysis reduces the tumor cell-secreted CCL2 levels

Given the essential role of HK2 in glycolysis and resultant protein lactylation, we generated a KPC cell line with knockdown of *Hk2* and used it for orthotopic mouse tumor model (39) (**Figure 1C and Supplementary Figure 3A**). Knockdown of *Hk2* significantly decreased ^{18}F-FDG uptake and tumor weight in vivo (**Figure 3, A and B**). Depletion of $CD8^+$ T cells from the mice partially offset the tumor-inhibiting effect (60% vs 27%) by Hk2 knockdown in comparison with the control mice (**Figure 3B and Supplementary**

Figure 3B). Glycolysis inhibition by *HK*2 knockdown had similar effects on the tumor immune microenvironment as observed in KRAS inhibition by MRTX1133, including decreased macrophage infiltration, and increased $CD8^+$ T cell infiltration and activity (**Figure 3C**).

Considering that elevated glycolysis increases macrophage infiltration and enhances pro-tumor functions, we reasoned that aberrant glycolysis in tumor cells may suppress T cell activity through macrophages. By using clodronate liposomes to eliminate macrophages from the mice bearing KPC tumors, we found that macrophage deletion significantly decreased tumor weight (**Figure 3D and Supplementary Figure 3C**). However, *Hk2* knockdown did not exert additional tumor suppression activity, suggesting that the immunological effect of glycolysis on tumor growth was mediated by tumor-infiltrated macrophages (**Figure 3D**). To examine how elevated glycolysis in tumors contributes to macrophage infiltration, we used bulk RNA-seq to identify glycolysis-dependent transcriptomics in KPC cells treated with or without 2-Deoxy-D-glucose (2-DG), a specific HK2 inhibitor. Among the most significantly altered genes (Log FC<-1.5, p adjusted<0.05, base mean>500), CCL2 is the only recognized chemokine for recruiting macrophages and monocytes (40) (**Figure 3E**). We found that knockdown of HK2 decreased CCL2 expression and secretion in KPC cells **(Supplementary Figure 3D)**. We also confirmed that treatment of 2-DG significantly reduced CCL2 expression in human PDAC cell lines, Panc02 and PANC-1, while supplementation of sodium lactate

(NALA), the end product of the glycolysis, increased CCL2 expression (**Figure 3F**). In line with the CCL2 expression levels, the secretion of CCL2 by tumor cells decreased when treated with 2-DG and increased when treated with NALA (**Figure 3G**). As a control, *Csf1*, another important monocyte/macrophage chemokine (41), was not significantly changed when treated with 2-DG or NALA **(Supplementary Figure 3E)**. We checked serum CCL2 levels in the previous cohort of 20 patients with high or low Pan-Kla levels. We found that the "Higher Pan-Kla" group had higher serum CCL2 levels (**Figure 3H and Supplementary Table 1**). In a cohort of PDAC patients with available serum samples and clinical outcome information, we found that high serum CCL2 levels was significantly correlated with poor overall survival (**Figure 3I and Supplementary Table 4**).

To determine whether CCL2 acts as a key factor in immunotherapy resistance, we analyzed the previously mentioned randomized clinical trial cohort for PDAC immunotherapy (3). We found that the serum CCL2 levels in non-responders was significantly higher than those in responders (**Figure 3J and Supplementary Table 3**). Serum CCL2 levels are closely related to immunotherapy outcomes, with an AUC value of 80.88 (specificity: 54.94; sensitivity:100 with cutoff 250.9756), using overall survival time as the outcome metric (**Figure 3K and Supplementary Table 3**). The results suggested that that PDAC patients with high serum CCL2 are more likely to develop immunotherapy resistance. In the orthotopic KPC mouse tumor model, immune

checkpoint blockade using anti-PD-1 mAb had minimal effect on tumor suppression. However, treatment with PF-4136309, a potent and selective CCR2 antagonist, drastically sensitized tumors to the anti-PD1 therapy (**Supplementary Figure 4A**). In line with this result, anti-PD-1 immunotherapy was more effective for the KPC tumors with *Hk2* knockdown, while PF-4136309 had no effect on the HK2-KD KPC tumors compared to the vehicle control treatment (**Supplementary Figure 4A**). Analysis of tumor-infiltrated lymphocytes revealed that knockdown of *Hk2* or inhibiting CCL2 signaling in KPC tumors reduced monocyte/macrophage infiltration but enhanced T cell infiltration and function (**Supplementary Figure 4B**). Collectively, these results demonstrated that inhibition of glycolysis sensitized PDAC to immunotherapy, with CCL2 acting as a key factor.

ENSA K63 lactylation upregulates STAT3-CCL2 signaling in tumor cells

In both bulk RNA-seq analyses of KPC cells treated with 2-DG or NALA, *Ccl2* was found significantly down-regulated or induced (**Figure 3E and Figure 4A**). Additionally, STAT3 is a transcriptional factor associated with lactate metabolism among most differentially expressed genes (16, 42) (**Figure 4A**). We also confirmed that NALA upregulated the activity of STAT3, indicated by its tyrosine 705 (Y705) phosphorylation level, while 2-DG downregulated the STAT3 phosphorylation (**Figure 4B and Supplementary Figure 5A**). The results were consistent with previous studies showing that CCL2 was transcriptionally regulated by STAT3 (43-45). Treatment of KPC cells with STAT3

inhibitor (STAT3-IN-11) decreased the mRNA level of *Ccl2*, and this effect was not restored by NALA treatment (**Figure 4C**). Previous studies have shown that cell-intrinsic glycolytic activity and extracellular uptake of lactate can regulate intracellular lactate levels accompanied with protein lactylation level(20, 23, 39). Considering that NALA did not significantly change the pH of the culture medium, lactate may act as a signaling molecule to regulate STAT3 phosphorylation. Lactylation is a dynamic process in a cell, and EP300 has been identified as a primary writer for both histone and non-histone lactylation (24). Treatment of KPC cells with a EP300 inhibitor (A-485), STAT3 phosphorylation was decreased, and this effect could not be restored by the addition of NALA (**Figure 4D and Supplementary Figure 5B**). To identify lactylated proteins that regulate STAT3 phosphorylation, we conducted proteomics analysis to search for lactylated proteins on both human pancreatic tumor samples (n=3) and mouse KPC cells. Out of 324 lactylated proteins identified in both human and mouse samples, three proteins– ENSA (endosulfine alpha), CKS1B (CDC28 protein kinase regulatory subunit 1B) and NUCKS1 (nuclear casein kinase and cyclin dependent kinase substrate 1) –are potential regulators for protein phosphorylation based on gene ontology analysis (**Supplementary Table 5**). Further validation showed that ENSA overexpression increased the phosphorylation of STAT3, but CKS1B or NUCKS overexpression did not (**Supplementary Figure 5C**). ENSA is a highly conserved cAMP-regulated phosphoprotein. We indeed confirmed lactylation of ENSA in KPC cells (**Figure 4E**). Previous studies revealed that inhibiting cellular glycolysis with 2-DG and mimicking

extracellular lactate uptake with NALA can regulate intracellular lactate levels, which could be used as a tool to regulate the overall level of protein lactylation(20, 23, 39). Treatment of KPC cells with 2-DG decreased ENSA lactylation and interaction with EP300, while treatment with NALA produced the opposite effects, supporting that EP300 was the writer of ENSA lactylation (**Figure 4E and Supplementary Figure 5D**). To confirm whether NALA or 2-DG regulated phosphorylation of STAT3 in an ENSA-dependent manner, we constructed an *Ensa*-KO KPC cell line and found that knockout of *Ensa* decreased phosphorylation of STAT3, and this effect could not be restored by NALA (**Figure 4F and Supplementary Figure 5E**).

Proteomics analysis with mass spectrometry identified multiple lactylation sites on ENSA, including K40, K56, K63, K74, and K80. To determine the key lactylation event for STAT3 signaling, we mutated each lactylation sites from lysine to arginine (K to R) on ENSA. While overexpression of ENSA-WT, ENSA-K40R, ENSA-K56R, ENSA-K74R, and ENSA-K80R in *Ensa*-KO KPC cells upregulated phosphorylation of STAT3, ENSA-K63R overexpression did not (**Figure 4, G and H and Supplementary Figure 5F**). To better quantify the differences, we conducted an ELISA experiment to measure pSTAT3 levels. We found that the pSTAT3 level in cells overexpressing ENSA-K63R was comparable to the control group, while overexpression of ENSA-WT and other mutants led to a threefold increase in pSTAT3 levels (**Supplementary Figure 5G**).

Quantitative PCR revealed that *Ccl2* expression increased with ENSA-WT overexpression but not with ENSA-K63R overexpression (**Figure 4I**). These results demonstrated that ENSA K63 lactylation is a key event for STAT3-CCL2 signaling in pancreatic cancer cells.

ENSA is a protein phosphatase inhibitor that specifically inhibits protein phosphatase 2A (PP2A). In the cell, PP2A is a heterotrimeric complex that consists of a structural subunit A, a catalytic subunit C, and a regulatory subunit B. ENSA is known to physically interact with a regulatory subunit of PP2A, PP2A regulatory subunit B delta isoform (PPP2R2D), and thus inhibit the catalytic activity of PP2A (46). The interaction between ENSA and PPP2R2D was enhanced in KPC cells treated with NALA, whereas the interaction was weakened in the cells treated with 2-DG (**Figure 4J and Supplementary Figure 5H**). The results suggest that ENSA lactylation inhibits the PP2A activity by enhancing the ENSA-PPP2R2D interaction. We also identified SRC, an upstream tyrosine kinase for STAT3, as an interactor of the PP2A catalytic subunit, PPP2CA (PP2A catalytic subunit alpha) by mass spectrometry (**Supplementary Table 6**). The PPP2CA-SRC interaction was enhanced in KPC cells treated with 2-DG, whereas the interaction was weakened treated with NALA (**Figure 4K and Supplementary Figure 5I**)(47). This is consistent with previous reports that PP2A dephosphorylates SRC at S12 and decreases the kinase activity of SRC (48-51). To validate the kinase activity of SRC on STAT3, constitutive phosphorylation (S12D) and non-phosphorylation (S12A) mutants were

constructed to further investigate the function of S12 phosphorylation. The S12D mutation of SRC upregulated STAT3 Y705 phosphorylation, while the S12A mutation of SRC downregulated STAT3 Y705 phosphorylation (**Figure 4L and Supplementary Figure 5J**), highlight the importance of SRC S12 phosphorylation on its kinase activity. In a phosphatase assay, we tested the SRCpS12-specific phosphatase activity of PP2A in the KPC cells. The dephosphorylation activity of PP2A was decreased when the cells were treated with 2-DG, but increased upon NALA treatment (**Figure 4M**).

To demonstrate the ENSA-K63la/SRC-pS12/STAT3-pY705 signaling cascade, we generated antibodies that specifically identify ENSA-K63la or SRC-pS12. Western blotting analysis revealed that treatment with NALA upregulated ENSA-K63 lactylation, SRC-S12 phosphorylation, and STAT3-Y705 phosphorylation, while 2-DG downregulated ENSA-K63 lactylation, SRC-S12 phosphorylation, and STAT3-Y705 phosphorylation (**Figure 4N and Supplementary Figure 5K**) in both human and mouse PDAC cell lines. We also conducted relevant experiments using an LDHA inhibitor Sodium Oxamate(20). After treating KPC and PANC-1 cell lines with the previously reported dose of 20 μM for 24 hours, ENSA-K63la, SRC-pS12 and STAT3-pY705 level was significantly decreased while this effect was largely weakened by the addition of NALA (**Supplementary Figure 5, L-N**). Taken together, heightened glycolysis in pancreatic cancer cells causes lactate accumulation, leading to up-regulated protein lactylation. Particularly, ENSA-K63 lactylation inactivates PP2A, enhances SRC kinase

activity, and eventually increases STAT3 Y705 phosphorylation and boosts CCL2 secretion.

Design of a peptide inhibitor specifically targeting ENSA-K63la

We tested whether ENSA-K63 lactylation makes major contribution to an immunosuppressive TME in PDAC. To this end, we examined the orthotopic tumor growth and progression using mouse *Ensa*-KO KPC cells overexpressing wildtype (ENSA-WT) or K63 mutant ENSA (ENSA-K63R). Overexpression of ENSA-WT significantly increased tumor growth, while overexpression of ENSA-K63R did not (**Figure 5A**). Flow cytometric analysis revealed that overexpression of ENSA-WT markedly increased macrophage/monocyte infiltration but decreased $CD8^+$ T cell infiltration and function, similar to the effect of elevated glycolysis on the immunosuppressive microenvironment (**Figure 5, B and C and Supplementary Figure 6A**). Given its important role in pancreatic tumor progression, ENSA-K63la is thought as a potential therapeutic target. Previous studies have demonstrated that cell-penetrating peptides are a promising and effective approach to inhibit post-translational modification of target proteins (23). Because the amino acids in the vicinity of K63 are conserved in humans and mice, we designed five individual peptides as competitive inhibitors for inhibiting both human and mouse ENSA-K63la (**Figure 5D**). A cell-penetrating peptide (HLYVSPWGG) was added to N-terminus of each peptide inhibitor (23). Y705 phosphorylation of STAT3 was used as an indicator for the inhibitory activity of the

peptide inhibitors. After incubation with each peptide inhibitor (K63-pe) for 24h, KPC cells were tested for decreased Y705 phosphorylation of STAT3 (**Figure 5E**). Among the five peptide inhibitors, K63-pe inhibitor 3 exhibited the best inhibitory activity of STAT3 (IC50 = 5.797μM) in comparison with vehicle control and negative control K63la-pe-3 (**Figure 5, E and F**). In the orthotopic KPC tumor model, K63-pe-3 also showed great anti-tumor activity when used at the dose of 10 mg/kg every day with intraperitoneal (i.p.) injection (**Figure 5G**). Analysis of tumor infiltrating lymphocytes also demonstrated that monocytes, macrophages, and $ARG1^{+}$ macrophages were decreased and CD8+ T cells were increased with treatment of K63-pe (**Figure 5H and Supplementary Figure 6B**). In vivo experiments also revealed that K63-pe-3 sensitized anti-PD1 immunotherapy in the orthotopic KPC mouse model (**Figure 5I**).

Lactate accumulation reprograms TAMs by ENSA lactylation

Lactate, mainly produced by tumor cells through glycolysis, is secreted into the TME as a signaling molecule (52, 53). We have shown that elevated glycolysis not only increased macrophage infiltration but also promoted a pro-tumor signature (**Figure 1, G and H and Supplementary Figure 1, E and F**). In the microenvironment of KPC-derived mouse tumors, TAMs showed the highest levels of Pan-Kla and p-STAT3 among all the immunocytes (**Figure 6A**). *Hk2* knockdown in the tumor cells significantly decreased Pan-Kla and p-STAT3 levels in TAMs but not in other immunocytes, indicating that TAMs are the primary immune cells affected by tumor-derived lactate

(**Figure 6A**). We verified in vitro whether $CD8^+$ T cells, another important immune cell type in this study, are unable to upregulate their own lactylation modifications when stimulated by exogenous lactate. We also isolated naive $CD8^+$ T cells ($CD45^+CD3^+CD8^+CD25^-$) from the spleen. We found that when $CD8^+$ T cells were activated using anti-CD3/anti-CD8/IL-2 stimulation ($CD45^+CD3^+CD8^+CD25^+$), the overall Pan-Kla levels increased compared to naive $CD8^+$ T cells. However, these activated T cells ($CD45^+CD3^+CD8^+CD25^+$) were not affected by tumor-secreted lactate or additional NALA supplementation, with no significant changes in Pan-Kla levels. In contrast, for naive $CD8^+$ T cells ($CD45^+CD3^+CD8^+CD25^-$), tumor-secreted lactate increased the intracellular Pan-Kla levels. Moreover, naive $CD8^+$ T cells treated with the supernatant of HK2-NC KPC cells showed a more pronounced increase in intracellular Pan-Kla levels compared to those treated with the supernatant of HK2-KD KPC cells. Additionally, NALA supplementation also enhanced the intracellular Pan-Kla levels (**Supplementary Figure 7A**). These results were quite interesting. Previous studies reveal that in activated $CD8^+$ T cells with high glycolysis-derived intracellular lactate, extracellular lactate does not impact protein lactylation. However, in naive $CD8^+$ T cells with low glycolysis, extracellular lactate upregulates protein lactylation(54). Previous studies have revealed that TAMs demonstrate significant metabolic adaptability, enabling them to thrive in the tumor microenvironment(16, 55-57). TAMs often display a shift from glycolysis (characteristic of M1 macrophages) to oxidative phosphorylation and fatty acid oxidation (similar to M2 macrophages)(16, 55-57). This lactate derived from tumor cells

not only fuels their metabolic needs but also promotes an immunosuppressive phenotype. Overall, TAMs' metabolic plasticity enables them to respond to the dynamic conditions of the TME, fostering their pro-tumorigenic roles and contributing to immune evasion.

Using conditioned medium from control (*Hk2*-NC) and *Hk2*-KD KPC cell cultures to treat bone marrow-derived macrophages (BMDMs), we observed decreased levels of Pan-Kla, ENSA-K63 lactylation, SRC-S12 phosphorylation, and STAT3-Y705 phosphorylation in BMDMs when cultured with *Hk2*-KD KPC medium, compared to those BMDMs cultured with *Hk2*-NC KPC medium, and these reduced levels could be largely restored in the BMDMs cultured with NALA-treated *Hk2*-KD KPC medium (**Figure 6B and Supplementary Figure 7B**). We also found that treatment with K63-pe-3 inhibitor decreased ENSA-K63 lactylation, SRC-S12 phosphorylation, and STAT3-Y705 phosphorylation in BMDMs pretreated with KPC conditioned medium (**Figure 6C and Supplementary Figure 7C**). Collectively, these results suggest that tumor cell-derived lactate regulated the ENSA-K63la/SRC-pS12/STAT3-pY705 axis in TAMs.

A number of pro-tumor genes downstream of STAT3 signaling, including *Ccl2*, *Arg1*, *S100A9*, and *IL10*, were significantly upregulated in TAMs upon NALA treatment (58-61) (**Figure 6D**). Knocking down HK2 in KPC significantly reduced CCL2, ARG1, S100A9 and IL10 expression in macrophage in vivo (**Figure 6E**). Compared with BMDMs

cultured with *Hk2*-KD KPC medium, BMDMs cultured with *Hk2*-NC KPC medium also revealed higher expression levels of *Ccl2*, *Arg1*, *S100A9*, and *IL10*, which could be reduced when *Hk2*-NC KPC cells were treated with K63-pe-3 (**Supplementary Figure 7D**). We also found that BMDMs pretreated with *Hk2*-NC KPC medium had greater inhibitory activity on $CD8^+$ T cell proliferation compared with BMDMs cultured with *Hk2*-KD KPC medium, and this effect could be restored when *Hk2*-NC KPC cells were pretreated with K63-pe-3 (**Supplementary Figure 7E**). Multiplex IHC staining of paraffin sections of pancreatic tumor tissues from patients and genetically modified KTC mice showed that tumor tissues with overall higher scores of Pan-Kla had higher Pan-Kla levels in macrophages, suggesting that lactate accumulated in the microenvironment impacts Pan-Kla levels in TAMs (**Figure 6, F and G and Supplementary Figure 7, F and G**). As expected, Pan-Kla levels in TAMs were positively correlated with the levels of CCL2, ARG1, S100A9, and p-STAT3 (**Figure 6, F and G and Supplementary Figure 7, F and G**).

Overall, the tumor cells' autonomously enhanced glycolysis and protein lactylation modification upregulate CCL2 expression through the ENSA-K63la/SRC-pS12/STAT3-pY705 axis, thereby recruiting macrophages. The lactate secreted by the tumor further affects the infiltrating macrophages and promotes pro-tumoral signature. Collectively, tumor cell intrinsic lactate production and paracrine lactate lead to the enrichment of immunosuppressive macrophages in the microenvironment.

ENSA-K63la/STAT3-pY705/CCL2 axis is a therapeutic target in PDAC

We further investigated the clinicopathological correlation of ENSA-K63la in PDAC using a tissue microarray of specific antibodies in mIHC assays. The results demonstrated that ENSA-K63la levels were positively correlated with STAT3-pY705 levels in human PDAC (**Figure 7, A and B**). Furthermore, high levels of ENSA-K63la and STAT3-pY705 were associated with poor overall survival of PDAC patients (**Figure 7, C and D**).

To assess the potential translational value of K63-peptide inhibitor and CCR2 inhibitor, a human $CD34^+$ hematopoietic stem cell (HSC)-transplanted NCG mouse model with patient-derived xenografts (PDX) was used (**Figure 7E**). Treatment with CCR2i or K63-pe-3 significantly decreased tumor growth and enhanced the efficacy of anti-PD1 immune checkpoint blockade therapy in the humanized PDX models (**Figure 7F**). Tumor immune profiling analysis revealed that treatment with CCR2i and K63-pe decreased macrophage and monocyte infiltration and increase $CD8^+$ T cell infiltration (**Figure 7G**). In addition, activated $CD8^+$ T cells ($CD25^+$) were increased and exhausted $CD8^+$ T cells ($CD366^+$) were decreased with both the treatments (**Figure 7G**). Taken together, CCR2i or K63-pe is a promising therapeutic approach used in combination therapy with immune checkpoint blockade in treating PDAC.

Since ENSA-K63-pe, CCR2i and MRTX1133 can reshape the immune microenvironment of pancreatic cancer and enhance T cell infiltration and function, we

tested whether these drugs have the ability to broadly sensitize tumors to immunotherapy (**Figure 2, Supplementary Figure 4, Figure 5, Supplementary Figure 6 and Figure 7**). We found that these drugs could sensitize tumors to anti-CTLA-4 immunotherapy as well, not just to anti-PD1 therapy (**Supplementary Figure 8A**).

In conclusion, elevated glycolysis level in PDAC promotes ENSA-K63la, a crucial step that triggers STAT3-CCL2 signaling in tumor cells. Elevated CCL2 secretion by tumor cells facilitates tumor-associated TAM recruitment to the TME. Tumor-derived lactate drives transcriptional reprogramming (CCL2, ARG1, IL10, S100A9) in TAMs via ENSA-K63la/STAT3-pY705 axis, promoting an immunosuppressive environment and immunotherapy resistance. Targeting mutant-KRAS, CCL2, or ENSA-K63la enhances the efficacy of immune checkpoint blockade therapy in pancreatic tumor models. In addition, 18F-FDG uptake, pathological biopsy samples Pan-Kla expression and serum CCL2 level in patients could predict clinical outcomes in immunotherapy.

Discussion

The overall response rate of immunotherapy in PDAC is relative low compared with other tumors (1). The unique genomic landscape and environmental features of pancreatic cancer result in different response to immunotherapy. Identifying patients who are sensitive to anti-PD immunotherapy and developing combination therapies for those who may not respond is an urgent problem to be solved.

Elevated glycolysis significantly alters the tumor microenvironment. In this study, we demonstrate that the glycolytic process and its derivative, lactylation modification, possess potential prognostic value in the context of immunochemotherapy. Utilizing ^{18}F-FDG PET-CT to image glycolysis intensity, we reviewed a prospective cohort of pancreatic cancer patients who underwent ^{18}F-FDG PET-CT prior to chemotherapy or immunochemotherapy. Patients were stratified into two groups based on SUVmax (35). Our findings indicate that patients with hyper-glycolysis (higher ^{18}F-FDG uptake) exhibited a poor response to immunochemotherapy. While ^{18}F-FDG PET-CT is typically employed to identify recurrence and metastasis, it is rarely used for initial diagnosis. Therefore, we considered paracentesis, which is more commonly employed in the initial diagnosis of pancreatic cancer. We assessed Pan-Kla expression in biopsy specimens using multiplex immunohistochemistry. A retrospective review of a previous RCT cohort revealed that patients with high Pan-Kla expression had poor survival outcomes

following immunochemotherapy (3). Pan-Kla expression may serve as a predictor of immunotherapy efficacy, with an AUC of approximately 95.59.

We identified a glycolysis-dependent ENSA-K63la/SRC-pS12/STAT3-pY705 axis that promotes an immunosuppressive microenvironment. Based on this, we propose three potential targeted intervention strategies. Firstly, targeting the aberrant glycolysis enhancements caused by KRAS mutations could be effective. Using the KRAS-G12D inhibitor MRTX1133 significantly reduced glycolysis and tumor weight in vivo. Given that KRAS mutations are absent in normal cells, targeting mutant KRAS offers significant specificity and clinical potential. Secondly, ENSA-K63la could serve as a potential target. ENSA-K63 can undergo lactylation, inactivating PP2A, sustaining SRC-S12 phosphorylation, and promoting STAT3 constitutive activation. A cell-penetrating peptide designed to block ENSA-K63la could reduce STAT3-Y705 phosphorylation. This K63-peptide could potentially reshape the tumor microenvironment and enhance the sensitivity of pancreatic cancer to immunotherapy. Finally, pharmacologically targeting CCR2 might be a universal strategy for combination therapy. Our study found that serum CCL2 levels negatively correlate with overall survival and are associated with poor immunochemotherapy outcomes. Elevated tumor glycolysis attracts monocytes/macrophages via the ENSA-K63la/SRC-pS12/STAT3-pY705/CCL2 axis. Macrophages in the tumor microenvironment uptake lactate derived from the tumor, which further promotes the ENSA-K63la/SRC-pS12/STAT3-pY705 axis and increases

CCL2 expression, enhancing the chemotactic effect on monocytes/macrophages. Additionally, STAT3 activation promotes the expression of CCL2, ARG1, S100A9, and IL10, contributing to an immunosuppressive microenvironment. Blocking the CCL2/CCR2 axis could reduce macrophage infiltration and inhibit the formation of pro-tumor macrophages.

Radiology, pathology, serology, and genomics serve as pivotal pillars in achieving precision therapy. Techniques such as 18F-FDG PET/CT and Pan-Kla staining on biopsy samples allow for the identification of patients who may respond well to immunotherapy. Serological assessments can reveal individuals who might benefit from CCR2 inhibition. Additionally, genomic profiling can detect patients harboring specific KRAS mutations, making them ideal candidates for targeted therapies. By leveraging these advanced diagnostic tools, healthcare providers can tailor precise treatment plans to the unique genetic, metabolic, and molecular profiles of each patient, thereby optimizing therapeutic outcomes.

This study has several limitations. Although sodium lactate supplementation can largely restore the downregulation of STAT3 phosphorylation caused by glycolysis inhibition, other factors in the glycolytic process may also influence STAT3 activation. Additionally, while ENSA-K63la is a key regulator of STAT3 activation, lactate may activate STAT3

phosphorylation through other pathways. In the future, we will further investigate the impact of glycolysis on the immune microenvironment of pancreatic cancer.

Methods

Sex as a biological variable

We used male mice to perform animal experiments. Since estrogen could be a suppressive factor in tumor progression, male mice could be a universal model for cancer therapy. Both men and women were included in the clinical cohorts, and there was no bias in the grouping, and there were consistent results for both men and women.

Human tissues and patient cohorts

Paraffin-embedded PDAC tissue array slides were created by Wuhan Servicebio technology using in-house PDAC tissue specimens. Additionally, four patient cohorts were used in this research. Clinical data was shown in **Supplementary Table 1-4**.

PET/CT Imaging

18F-FDG PET-CT scans were conducted using a PET/CT scanner (Siemens Healthineers). Image analysis followed the same methodology as previous studies(35). Standardized Uptake Value (SUV) was utilized to normalize tissue activity concentration, injected dose, and body weight. The SUVmax was used for analysis in this study.

Cell culture

The KPC cell line was a kind gift from the laboratory of Prof. Raghu Kalluri. All other PDAC cell lines were purchased from ATCC.

Bone marrow-derived macrophages (BMDM) were obtained from C57BL/6 mice and cultured in RPMI Medium containing M-CSF (40 ng/ml), 10% fetal bovine serum, and 1% penicillin and streptomycin at 37°C with 5% CO2. After approximately three days, once the cells were adherent, fresh RPMI complete medium containing KPC supernatant was added to induce tumor-associated macrophages, with a ratio of 1:1 for KPC supernatant to RPMI medium.

Plasmid and cell transfection

Hk2 short hairpin RNA was cloned into the pLKO.1-EGFP plasmid, while Ensa small guide RNA was cloned into the LentiCRISPRV2-GFP plasmid. Other plasmids used in this research were purchased from industry.

To create an *Ensa* knockout subclone, the LentiCRISPRV2-GFP plasmid was transiently transfected into KPC cell line, which were then sorted into single cells using green fluorescent protein (GFP) cytometry and placed into 96-well plates. For stable transfection cell lines, lentivirus was used following the method that described in previous studies(62). All transient and stable transfections were confirmed via western blotting.

Animal experiments

Six-week-old male mice were each challenged by 1000000 KPC cells in a mixture of medium and matrigel (1:1) in all experiments. As for orthotopic tumor model, KPC cells in 25 μl mixture was injected into the pancreas under anesthesia.

HuCD34+HSC-NOD/ShiLtJGpt-Prkdc^{em26Cd52}Il2rg^{em26Cd22}/Gpt(CH) mice were purchased from GemPharmatech Co., Ltd. To generate Patient-Derived Xenograft (PDX) models, fresh tumor samples from patients during surgery were collected. A tumor fragment was inserted into the pocket created under the skin of a nude mice. Tumor growth was monitored and once the tumor reached the desired size, the mouse was euthanized for tumor collection. Under sterile conditions, the tumor tissue was trimmed into small fragments (2-3 mm^3) using sterile scissors or scalpels and then transplanted into NCG mice. Tumor growth was monitored and the mouse was euthanized for tumor collection. The samples were mechanically dissociated into small fragments using scissors and scalpels, then placed in DMEM supplemented with 2% FBS, collagenase IV (1 mg/ml), DNase (10 μg/ml), and EDTA (2 mM). They were incubated at 37°C with shaking at 200 rpm for 30 minutes. Digestion was terminated by adding DMEM containing 10% FBS. The dissociated tissues were then filtered through a 40-μm cell strainer and washed with PBS. The tumor cells were resuspended in a mixture of PBS and Matrigel (1:1, 1000000 cells in 25 μl mixture) and injected into the franks of *HuCD34+HSC-NOD/ShiLtJGpt-Prkdc^{em26Cd52}Il2rg^{em26Cd22}/Gpt(CH)* mice.

Doses of pharmacological treatment used in the study were listed as follows: anti-PD1mAb (100 μg/mouse, i.p., tid), anti-CD8mAb (100 μg/mouse, i.p., tid), Clodronate Liposomes (i.p, q7d), MRTX1133 (0.2 mg/mouse, i.p., qd), PF-4136309 (0.2 mg/mouse, i.p., qd) and cell-penetrating peptide (0.2 mg/mouse, i.p., qd). Tthe mice were sacrificed, and the tumors were excised for weighing and further analysis. All of mice which were alive were included in data analysis.

Flow cytometry

Sample pretreatment was the same as previous studies(62). Samples were detected using a Fortessa flow cytometer (Becton Dickinson, Franklin Lakes, NJ, USA) and Cytek Aurora (Cytek Biosciences, Shanghai, China). Full spectrum flow cytometry was performed as guided(63). Data were analyzed using FlowJo software (Becton Dickinson, version 10.8.1).

Western blotting and immunoprecipitation

Cells and tissues were lysed using radioimmunoprecipitation assay (RIPA) buffer containing a protease inhibitor cocktail and a phosphatase inhibitor cocktail. For immunoprecipitation, cell supernatants collected after treatment were incubated with anti-FLAG, anti-HA, or anti-MYC magnetic beads for 4 hours. All experiments were conducted following protocols from previous studies(62). The grayscale values of the

WB bands were quantified using ImageJ. The relative expression was normalized to control group.

Quantitative real-time reverse transcription-PCR analysis

Cell total RNA was isolated and then reversed transcribed. Primers used were shown in **Supplementary Table 7**. The relative expression was normalized to that of ACTB/*Actb* (encoding beta actin) using the 2−ΔΔCt method.

Multiplex Immunohistochemistry

Multiplex IHC was performed using an Opal Polaris 7-Color Manual IHC Kit (NEL861001KT) following the provided protocol strictly. For follow-up quantitative analysis, InForm software (version 2.5; Akoya Biosciences, Menlo Park, CA, USA) was used. Cells were adaptively segmented based on nuclear, cytoplasm and cell membrane markers. Cells were marked to develop a training classifier and then phenotype using machine learning. The proportion of each cell type in all cells was calculated. The histochemistry score (H-score) of the total region were calculated. The mean fluorescence intensity of each cell type could be calculated. As for TMA, incomplete regions were excluded in analysis. Tumor regions where proportion of tumor cells was less than 10% were excluded in analysis.

ELISA Assay

The concentration of CCL2 in serum or supernatant was quantified using an Elisa kit according to the manufacturer's instruction. The numbers of the cells and the volume of the liquid were kept consistent.

PP2A active enzyme quantification assay

SRC-pS12 cell-penetrating peptide (HLYVSPWGG-SKPKDApSQRRRSL) was incubated in KPC cell line for 24 hours before the test. Cellular protein phosphatase 2A (PP2A) active enzyme quantification assay kit was used to perform this study.

RNA-seq analysis

All samples were pretreated and analyzed by Biomedical Big Data Center of the First Affiliated Hospital, School of Medicine, Zhejiang University. The raw data that passed quality control was subjected to differential expression and functional enrichment.

Peptide synthesis

All peptides were synthesized by Guoping Pharmaceutic Inc (Hefei, China). The peptides used were all D isoforms, acetylated at the N-terminus and amidated at the C-terminus. The HLYVSPWGG sequence was used to enhance cell penetration. Peptides were dissolved in PBS for use.

Proteomics

To identify protein lactylated, proteins from PDAC samples and KPC cell lines were isolated, trypsinized, and labeled with TMT. Enrichment was performed using anti-L-lactyllysine antibody-conjugated agarose beads.

To identify protein interaction, LC-MS analysis was performed as previous reported(62).

Bioinformatics analysis

Considering the main differences focused on macrophages and T cells, we combined four public single-cell RNA sequencing datasets (CRA001160, GSE205013, GSE212966, phs002371). After integration with scVI and annotation with typical markers (CD3D, CD3E for T cells; CD68, CD14, CD163, LYZ, MRC1, S100A9 for myeloid cells), 348,560 cells remained in primary tumor samples without any treatment(64). Next, myeloid and T cell subsets were further identified into four and five types, respectively. The glycolysis score of the epithelial subset was calculated using ssGSEA, and patients were divided into two groups, glycolysis-high and glycolysis-low, based on the median average score(65). Grouped by patient classification, markers of macrophages and CD8+ T cells were identified using the FindAllMarkers function in Seurat (v5.0.1)(66). Markers with pct.1 > 0.05, log2FoldChange > 0.5, and adjusted P value < 0.01 were considered potential signatures. Gene Ontology (GO) enrichment was performed using clusterProfiler(67).

To explore functional differences between the two identified classes, GSEA was conducted using hallmark gene sets from the human collection of MSigDB (gsea-msigdb.org)(68-70). Additionally, ssGSEA in the GSVA package was used to assess glycolysis levels with a manually collected gene set (SLC2A1, HK2, GPI, PFK, PGK, PKM, LDHA, ENO1, PKM, LDHA, SLC16A3)(71). The resulting matrix (glycolysis_scores) contains glycolysis enrichment scores for each sample, which can be further analyzed or visualized.

Statistics

GraphPad Prism software (version 7.0; GraphPad Inc., La Jolla, CA, USA) was used for statistical analyses. Data from biological replicates are presented as the mean ± SD. Differences between two groups were compared using two-sided Student's t-tests, while one-way analysis of variance (ANOVA) was employed to analyze differences among three or more groups. Spearman's rank correlation was used to compare two variables. The Kaplan–Meier method and the Gehan–Breslow–Wilcoxon test was used to analyze differences between survival curves. ROC-AUC curves were utilized to evaluate the efficiency of predictive models. Throughout the study, a P value of < 0.05 was considered statistically significant.

Materials

Main regents and detailed information involved in this study was shown in **Supplementary Table 7**.

Study approval

Human samples and clinical information were collected from the Department of Hepatobiliary and Pancreatic Surgery at the First Affiliated Hospital, School of Medicine, Zhejiang University. No prospective patient cohort was included in this study. All medical records and biological samples were obtained from previous clinical treatments. The study is exempt from informed consent. The study protocol received approval from the Institutional Review Board of the First Affiliated Hospital, School of Medicine, Zhejiang University (IIT20240588A). Animal experiment received approval from the Institutional Review Board of the First Affiliated Hospital, School of Medicine, Zhejiang University.

Data availability

Raw RNA-seq data has been deposited to National Genomics Data Center (GSA Accession: CRA018166). Sequencing data are part of the HTAN dbGaP under accession phs002371.v3.p1. These data are available through the HTAN DCC Portal (https://data.humantumoratlas.org/) under the HTAN WUSTL Atlas. This paper does not include any original code. Source data are presented in “supporting data values” file.

Acknowledgments

This work was supported by grants from National Key Research and Development Program of China (2024YFA1306400 to XLB), the National Natural Science Foundation of

China (U20A20378, 82188102, and 81830089 to TBL; 82071867 and U23A20462 to XLB; 82403852 to XZZ; 82171721 and 81702376 to XZ), the Key Research and Development Program of Zhejiang Province (2019C03019 to TBL; 2020C03117 to XLB), “Ling Yan” Research and Development Program of Department of Zhejiang Province Science and Technology (2024C03167 to XLB) and China Postdoctoral Science Foundation [2024T170810 and 2024M752879 to XZZ]. We would like to thank PTM BIO, Cosmos Wisdom, Cifeng Cai, Univ Bio, Zhongyao Gao, Minghua Sun, Jianfeng Wang, Junyu Qiu, Lei Ni, Pengda Zou, Yahong Wu and Haoyu Tang for technical assistance.

Author contributions

K.S., X.Z. designed this research. K.S., X.Z., J.H., X.L., M.Y., K.S. supported methodology of this research. K.S., J.S., S.W., H.L., D.Z., L.Q., M.Y., C.L., M.L., L.H., J.S., N.L., Y.J., Y.C., S.Y., H.Y., L.L., X.L., J.L., Y.M., J.Z., Q.X., X.Z. performed the experiments. K.S., D.Z., J.H. visualized the results. X.B, T.L., X.Z., X.L. supervised this research. K.S., X.Z., X.B., X.L. wrote and revised this manuscript. K.S., X.Z., J.S., and

J.H. are co-first author; authorship order reflects the degree to which authors drove key developments in the work.

Inclusion and diversity

We support inclusive, diverse, and equitable conduct of research.

References

1. Hu ZI, and O'Reilly EM. Therapeutic developments in pancreatic cancer. *Nature reviews Gastroenterology & hepatology.* 2024;21(1):7-24.

2. Bear AS, Vonderheide RH, and O'Hara MH. Challenges and Opportunities for Pancreatic Cancer Immunotherapy. *Cancer cell.* 2020;38(6):788-802.

3. Fu Q, Chen Y, Huang D, Guo C, Zhang X, Xiao W, et al. Sintilimab Plus Modified FOLFIRINOX in Metastatic or Recurrent Pancreatic Cancer: The Randomized Phase II CISPD3 Trial. *Annals of surgical oncology.* 2023;30(8):5071-80.

4. Zhang J, Huang D, Saw PE, and Song E. Turning cold tumors hot: from molecular mechanisms to clinical applications. *Trends in immunology.* 2022;43(7):523-45.

5. Pavlova NN, and Thompson CB. The Emerging Hallmarks of Cancer Metabolism. *Cell metabolism.* 2016;23(1):27-47.

6. Dong LQ, Lu DY, Chen R, Lin YP, Zhu HW, Zhang Z, et al. Proteogenomic characterization identifies clinically relevant subgroups of intrahepatic cholangiocarcinoma. *Cancer cell.* 2022;40(1):70-+.

7. Bryant KL, Mancias JD, Kimmelman AC, and Der CJ. KRAS: feeding pancreatic cancer proliferation. *Trends BiochemSci.* 2014;39(2):91-100.

8. Kleeff J, Korc M, Apte M, La Vecchia C, Johnson CD, Biankin AV, et al. Pancreatic cancer. *Nat Rev Dis Primers.* 2016;2:22.

9. Habrook CJ, and Lyssiotis CA. Employing Metabolism to Improve the Diagnosis and Treatment of Pancreatic Cancer. *Cancer cell.* 2017;31(1):5-19.

10. Tao JX, Yang G, Zhou WC, Qiu JD, Chen GY, Luo WH, et al. Targeting hypoxic tumor microenvironment in pancreatic cancer. *J Hematol Oncol.* 2021;14(1):25.

11. Liu J, Liu Q, Zhang X, Cui M, Li T, Zhang Y, et al. Immune subtyping for pancreatic cancer with implication in clinical outcomes and improving immunotherapy. *Cancer cell international.* 2021;21(1):137.

12. DeNardo DG, and Ruffell B. Macrophages as regulators of tumour immunity and immunotherapy. *Nat Rev Immunol.* 2019;19(6):369-82.

13. Binnewies M, Roberts EW, Kersten K, Chan V, Fearon DF, Merad M, et al. Understanding the tumor immune microenvironment (TIME) for effective therapy. *Nature medicine.* 2018;24(5):541-50.

14. Zhu Y, Knolhoff BL, Meyer MA, Nywening TM, West BL, Luo JQ, et al. CSF1/CSF1R Blockade Reprograms Tumor-Infiltrating Macrophages and Improves Response to T-cell Checkpoint Immunotherapy in Pancreatic Cancer Models. *Cancer research.* 2014;74(18):5057-69.

15. Qin C, Yang G, Yang JS, Ren B, Wang HY, Chen GY, et al. Metabolism of pancreatic cancer: paving the way to better anticancer strategies. *Mol Cancer.* 2020;19(1):19.

16. Colegio OR, Chu NQ, Szabo AL, Chu T, Rhebergen AM, Jairam V, et al. Functional polarization of tumour-associated macrophages by tumour-derived lactic acid. *Nature.* 2014;513(7519):559-63.

17. Husain Z, Huang YN, Seth P, and Sukhatme VP. Tumor-Derived Lactate Modifies Antitumor Immune Response: Effect on Myeloid-Derived Suppressor Cells and NK Cells. *J Immunol.* 2013;191(3):1486-95.

18. Bader JE, Voss K, and Rathmell JC. Targeting Metabolism to Improve the Tumor Microenvironment for Cancer Immunotherapy. *Molecular cell.* 2020;78(6):1019-33.

19. Certo M, Tsai CH, Pucino V, Ho PC, and Mauro C. Lactate modulation of immune responses in inflammatory versus tumour microenvironments. *Nat Rev Immunol.* 2021;21(3):151-61.

20. Zhang D, Tang Z, Huang H, Zhou G, Cui C, Weng Y, et al. Metabolic regulation of gene expression by histone lactylation. *Nature.* 2019;574(7779):575-80.

21. Zong Z, Xie F, Wang S, Wu X, Zhang Z, Yang B, et al. Alanyl-tRNA synthetase, AARS1, is a lactate sensor and lactyltransferase that lactylates p53 and contributes to tumorigenesis. *Cell.* 2024;187(10):2375-92.e33.

22. Cheng Z, Huang H, Li M, and Chen Y. Proteomic analysis identifies PFKP lactylation in SW480 colon cancer cells. *iScience.* 2024;27(1):108645.

23. Chen Y, Wu J, Zhai L, Zhang T, Yin H, Gao H, et al. Metabolic regulation of homologous recombination repair by MRE11 lactylation. *Cell.* 2024;187(2):294-311.e21.

24. Shang S, Liu J, and Hua F. Protein acylation: mechanisms, biological functions and therapeutic targets. *Signal transduction and targeted therapy.* 2022;7(1):396.

25. Wu X, and Tao WA. Uncovering ubiquitous protein lactylation. *Nature methods.* 2022;19(7):793-4.

26. Chen M, Cen K, Song Y, Zhang X, Liou YC, Liu P, et al. NUSAP1-LDHA-Glycolysis-Lactate feedforward loop promotes Warburg effect and metastasis in pancreatic ductal adenocarcinoma. *Cancer letters.* 2023;567:216285.

27. Huang H, Wang S, Xia H, Zhao X, Chen K, Jin G, et al. Lactate enhances NMNAT1 lactylation to sustain nuclear NAD(+) salvage pathway and promote survival of pancreatic adenocarcinoma cells under glucose-deprived conditions. *Cancer letters.* 2024;588:216806.

28. Li F, Si W, Xia L, Yin D, Wei T, Tao M, et al. Positive feedback regulation between glycolysis and histone lactylation drives oncogenesis in pancreatic ductal adenocarcinoma. *Mol Cancer.* 2024;23(1):90.

29. Vander Heiden MG, Cantley LC, and Thompson CB. Understanding the Warburg effect: the metabolic requirements of cell proliferation. *Science (New York, NY).* 2009;324(5930):1029-33.

30. Zou C, Wang Y, and Shen Z. 2-NBDG as a fluorescent indicator for direct glucose uptake measurement. *Journal of biochemical and biophysical methods.* 2005;64(3):207-15.

31. Peng J, Sun BF, Chen CY, Zhou JY, Chen YS, Chen H, et al. Single-cell RNA-seq highlights intra-tumoral heterogeneity and malignant progression in pancreatic ductal adenocarcinoma. *Cell research.* 2019;29(9):725-38.

32. Chen K, Wang Y, Hou Y, Wang Q, Long D, Liu X, et al. Single cell RNA-seq reveals the CCL5/SDC1 receptor-ligand interaction between T cells and tumor cells in pancreatic cancer. *Cancer letters.* 2022;545:215834.

33. Werba G, Weissinger D, Kawaler EA, Zhao E, Kalfakakou D, Dhara S, et al. Single-cell RNA sequencing reveals the effects of chemotherapy on human pancreatic adenocarcinoma and its tumor microenvironment. *Nature communications.* 2023;14(1):797.

34. Rozenblatt-Rosen O, Regev A, Oberdoerffer P, Nawy T, Hupalowska A, Rood JE, et al. The Human Tumor Atlas Network: Charting Tumor Transitions across Space and Time at Single-Cell Resolution. *Cell.* 2020;181(2):236-49.

35. Li X, Lu N, Lin L, Chen Y, Yang S, Wang H, et al. (18)F-FAPI-04 Outperforms (18)F-FDG PET/CT in Clinical Assessments of Patients with Pancreatic Adenocarcinoma. *Journal of nuclear medicine : official publication, Society of Nuclear Medicine.* 2024;65(2):206-12.

36. Ying H, Kimmelman AC, Lyssiotis CA, Hua S, Chu GC, Fletcher-Sananikone E, et al. Oncogenic Kras maintains pancreatic tumors through regulation of anabolic glucose metabolism. *Cell.* 2012;149(3):656-70.

37. Wang XL, Allen S, Blake JF, Bowcut V, Briere DM, Calinisan A, et al. Identification of MRTX1133, a Noncovalent, Potent, and Selective KRAS^{G12D} Inhibitor. *J Med Chem.* 2021:11.

38. Tajiknia V, El-Deiry W, Schwermann MP, Zhou LL, and Huntington K. Combination of 5-Fluorouracil or ONC212 plus KRAS G12D inhibitor MRTX1133 against colorectal and pancreatic cancer cells results in immune-stimulatory cytokine patterns and unexpected synergies independent of G12D mutation. *Cancer research.* 2023;83(7):2.

39. Rho H, Terry AR, Chronis C, and Hay N. Hexokinase 2-mediated gene expression via histone lactylation is required for hepatic stellate cell activation and liver fibrosis. *Cell metabolism.* 2023;35(8):1406-+.

40. Deshmane SL, Kremlev S, Amini S, and Sawaya BE. Monocyte chemoattractant protein-1 (MCP-1): an overview. *Journal of interferon & cytokine research : the official journal of the International Society for Interferon and Cytokine Research.* 2009;29(6):313-26.

41. Zhu Y, Knolhoff BL, Meyer MA, Nywening TM, West BL, Luo J, et al. CSF1/CSF1R blockade reprograms tumor-infiltrating macrophages and improves response to T-cell checkpoint immunotherapy in pancreatic cancer models. *Cancer research.* 2014;74(18):5057-69.

42. Yang X, Lu Y, Hang J, Zhang J, Zhang T, Huo Y, et al. Lactate-Modulated Immunosuppression of Myeloid-Derived Suppressor Cells Contributes to the Radioresistance of Pancreatic Cancer. *Cancer immunology research.* 2020;8(11):1440-51.

43. Yang X, Lin Y, Shi Y, Li B, Liu W, Yin W, et al. FAP Promotes Immunosuppression by Cancer-Associated Fibroblasts in the Tumor Microenvironment via STAT3-CCL2 Signaling. *Cancer research.* 2016;76(14):4124-35.

44. Tsuyada A, Chow A, Wu J, Somlo G, Chu P, Loera S, et al. CCL2 mediates cross-talk between cancer cells and stromal fibroblasts that regulates breast cancer stem cells. *Cancer research.* 2012;72(11):2768-79.

45. Chun E, Lavoie S, Michaud M, Gallini CA, Kim J, Soucy G, et al. CCL2 Promotes Colorectal Carcinogenesis by Enhancing Polymorphonuclear Myeloid-Derived Suppressor Cell Population and Function. *Cell reports.* 2015;12(2):244-57.

46. Mochida S, Maslen SL, Skehel M, and Hunt T. Greatwall phosphorylates an inhibitor of protein phosphatase 2A that is essential for mitosis. *Science (New York, NY).* 2010;330(6011):1670-3.

47. Garcia R, Bowman TL, Niu G, Yu H, Minton S, Muro-Cacho CA, et al. Constitutive activation of Stat3 by the Src and JAK tyrosine kinases participates

in growth regulation of human breast carcinoma cells. *Oncogene.* 2001;20(20):2499-513.

48. Abbasian N, Bevington A, Burton JO, Herbert KE, Goodall AH, and Brunskill NJ. Inorganic Phosphate (Pi) Signaling in Endothelial Cells: A Molecular Basis for Generation of Endothelial Microvesicles in Uraemic Cardiovascular Disease. *International journal of molecular sciences.* 2020;21(19).

49. Pechkovsky A, Lahav M, Bitman E, Salzberg A, and Kleinberger T. E4orf4 induces PP2A- and Src-dependent cell death in Drosophila melanogaster and at the same time inhibits classic apoptosis pathways. *Proceedings of the National Academy of Sciences of the United States of America.* 2013;110(19):E1724-33.

50. Eichhorn PJ, Creyghton MP, Wilhelmsen K, van Dam H, and Bernards R. A RNA interference screen identifies the protein phosphatase 2A subunit PR55gamma as a stress-sensitive inhibitor of c-SRC. *PLoS genetics.* 2007;3(12):e218.

51. Yokoyama N, and Miller WT. Inhibition of Src by direct interaction with protein phosphatase 2A. *FEBS letters.* 2001;505(3):460-4.

52. Li Z, Wang Q, Huang X, Yang M, Zhou S, Li Z, et al. Lactate in the tumor microenvironment: A rising star for targeted tumor therapy. *Frontiers in nutrition.* 2023;10:1113739.

53. Wang Z, Dai Z, Zhang H, Liang X, Zhang X, Wen Z, et al. Tumor-secreted lactate contributes to an immunosuppressive microenvironment and affects CD8 T-cell infiltration in glioblastoma. *Frontiers in immunology.* 2023;14:894853.

54. Raychaudhuri D, Singh P, Chakraborty B, Hennessey M, Tannir AJ, Byregowda S, et al. Histone lactylation drives CD8(+) T cell metabolism and function. *Nature immunology.* 2024;25(11):2140-51.

55. Biswas SK, and Mantovani A. Orchestration of metabolism by macrophages. *Cell metabolism.* 2012;15(4):432-7.

56. Noy R, and Pollard JW. Tumor-associated macrophages: from mechanisms to therapy. *Immunity.* 2014;41(1):49-61.

57. Cheng S, Li Z, Gao R, Xing B, Gao Y, Yang Y, et al. A pan-cancer single-cell transcriptional atlas of tumor infiltrating myeloid cells. *Cell.* 2021;184(3):792-809.e23.

58. Qian BZ, Li J, Zhang H, Kitamura T, Zhang J, Campion LR, et al. CCL2 recruits inflammatory monocytes to facilitate breast-tumour metastasis. *Nature.* 2011;475(7355):222-5.

59. Qualls JE, Neale G, Smith AM, Koo MS, DeFreitas AA, Zhang H, et al. Arginine usage in mycobacteria-infected macrophages depends on autocrine-paracrine cytokine signaling. *Science signaling.* 2010;3(135):ra62.

60. Gao S, Mao F, Zhang B, Zhang L, Zhang X, Wang M, et al. Mouse bone marrow-derived mesenchymal stem cells induce macrophage M2 polarization through the nuclear factor-κB and signal transducer and activator of transcription 3 pathways. *Experimental biology and medicine (Maywood, NJ).* 2014;239(3):366-75.

61. Cheng P, Corzo CA, Luetteke N, Yu B, Nagaraj S, Bui MM, et al. Inhibition of dendritic cell differentiation and accumulation of myeloid-derived suppressor cells in cancer is regulated by S100A9 protein. *The Journal of experimental medicine.* 2008;205(10):2235-49.

62. Sun K, Zhang XZ, Lao MY, He LH, Wang SC, Yang HS, et al. Targeting leucine-rich repeat serine/threonine- protein kinase 2 sensitizes pancreatic ductal adenocarcinoma to anti-PD-L1 immunotherapy. *Molecular Therapy.* 2023;31(10):2929-47.

63. Park LM, Lannigan J, and Jaimes MC. OMIP-069: Forty-Color Full Spectrum Flow Cytometry Panel for Deep Immunophenotyping of Major Cell Subsets in Human Peripheral Blood. *Cytometry Part A : the journal of the International Society for Analytical Cytology.* 2020;97(10):1044-51.

64. Lopez R, Regier J, Cole MB, Jordan MI, and Yosef N. Deep generative modeling for single-cell transcriptomics. *Nature methods.* 2018;15(12):1053-8.

65. Barbie DA, Tamayo P, Boehm JS, Kim SY, Moody SE, Dunn IF, et al. Systematic RNA interference reveals that oncogenic KRAS-driven cancers require TBK1. *Nature.* 2009;462(7269):108-12.

66. Hao Y, Stuart T, Kowalski MH, Choudhary S, Hoffman P, Hartman A, et al. Dictionary learning for integrative, multimodal and scalable single-cell analysis. *Nature biotechnology.* 2024;42(2):293-304.

67. Wu T, Hu E, Xu S, Chen M, Guo P, Dai Z, et al. clusterProfiler 4.0: A universal enrichment tool for interpreting omics data. *Innovation (Cambridge (Mass)).* 2021;2(3):100141.

68. Subramanian A, Tamayo P, Mootha VK, Mukherjee S, Ebert BL, Gillette MA, et al. Gene set enrichment analysis: a knowledge-based approach for interpreting genome-wide expression profiles. *Proceedings of the National Academy of Sciences of the United States of America.* 2005;102(43):15545-50.

69. Mootha VK, Lindgren CM, Eriksson KF, Subramanian A, Sihag S, Lehar J, et al. PGC-1alpha-responsive genes involved in oxidative phosphorylation are coordinately downregulated in human diabetes. *Nature genetics.* 2003;34(3):267-73.

70. Liberzon A, Birger C, Thorvaldsdóttir H, Ghandi M, Mesirov JP, and Tamayo P. The Molecular Signatures Database (MSigDB) hallmark gene set collection. *Cell systems.* 2015;1(6):417-25.

71. Hänzelmann S, Castelo R, and Guinney J. GSVA: gene set variation analysis for microarray and RNA-seq data. *BMC bioinformatics.* 2013;14:7.

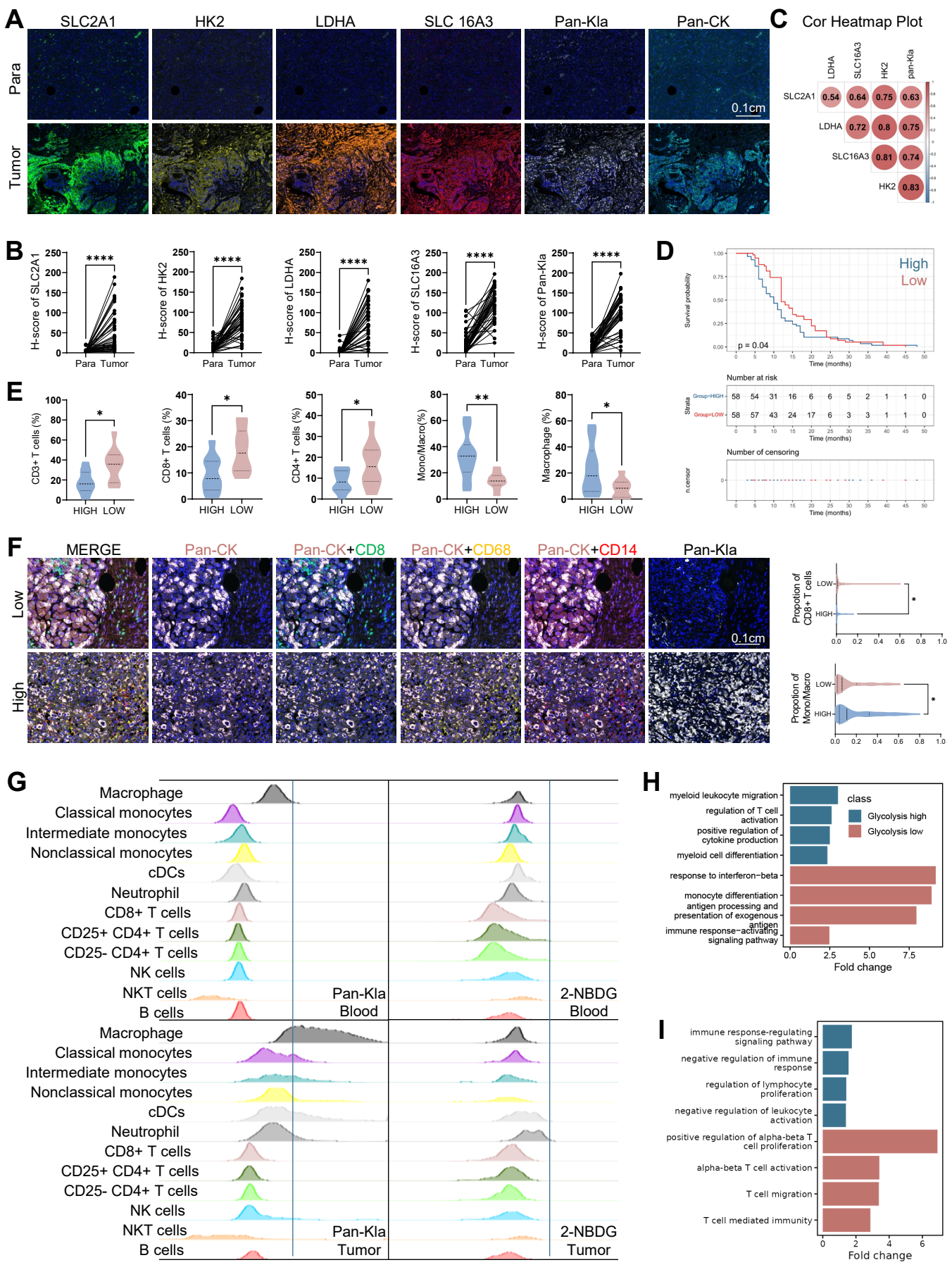
A
SLC2A1
HK2
LDHA
SLC 16A3
Pan-Kla
Pan-CK
Para
Tumor
0.1cm
C
Cor Heatmap Plot
LDHA
SLC16A3
HK2
pan-Kla
SLC2A1
0.54
0.64
0.75
0.63
LDHA
0.72
0.8
0.75
SLC16A3
0.81
0.74
HK2
0.83
B
H-score of SLC2A1
H-score of HK2
H-score of LDHA
H-score of SLC16A3
H-score of Pan-Kla
****
Para Tumor
D
High
Low
Survival probability
p = 0.04
Time (months)
Number at risk
Group=HIGH
Group=LOW
Strata
Number of censoring
n.censor
E
CD3+ T cells (%)
CD8+ T cells (%)
CD4+ T cells (%)
Mono/Macro(%)
Macrophage (%)
HIGH LOW
F
MERGE
Pan-CK
Pan-CK+CD8
Pan-CK+CD68
Pan-CK+CD14
Pan-Kla
Low
High
0.1cm
Propotion of CD8+ T cells
Propotion of Mono/Macro
LOW
HIGH
G
Macrophage
Classical monocytes
Intermediate monocytes
Nonclassical monocytes
cDCs
Neutrophil
CD8+ T cells
CD25+ CD4+ T cells
CD25- CD4+ T cells
NK cells
NKT cells
B cells
Pan-Kla Blood
2-NBDG Blood
Pan-Kla Tumor
2-NBDG Tumor
H
myeloid leukocyte migration
regulation of T cell activation
positive regulation of cytokine production
myeloid cell differentiation
response to interferon−beta
monocyte differentiation
antigen processing and presentation of exogenous antigen
immune response−activating signaling pathway
class
Glycolysis high
Glycolysis low
Fold change
I
immune response-regulating signaling pathway
negative regulation of immune response
regulation of lymphocyte proliferation
negative regulation of leukocyte activation
positive regulation of alpha-beta T cell proliferation
alpha-beta T cell activation
T cell migration
T cell mediated immunity
Fold change

Figure Legends

Figure 1. Elevated lactylation is correlated with immunosuppressive TME in PDAC. **A,** Representative images of multiplex immunohistochemistry (mIHC) staining in paracancerous (Para) and tumor tissues. Paracancerous and tumor tissues on tissue microarray were stained. Scale bar = 0.1cm. **B**, Expression differences of indicated genes between paracancerous and tumor tissues. Histochemistry score (h-score) was used to measure the expression of these genes in each region. Intact tissues were included in follow-up analysis. Statistical analyses were performed with the paired sample t test (41 pairs). **C,** Correlation analysis between SLC2A1, HK2, LDHA, SLC16A3 and Pan-Kla levels. 41 pairs of paracancerous and tumor tissues were included in the analysis. H-score was used to measure the expression of these genes in each region and then perform Pearson correlation analysis (n=82). **D**, Kaplan-Meier survival curves of overall survival (OS) for patients with PDAC in an in-house TMA. TMAs were stained using anti-Pan-Kla antibodies. Patients were divided into two groups according to median amount of h-score. Intact tumor tissues with survival data were included in follow-up analysis. Statistical analyses were performed with Log-rank (n=116). **E**, 20 fresh pancreatic tumor samples were process into a single-cell suspension and performed flow cytometry using Cytek. Samples were divided into two groups according to Pan-Kla expression. Statistical analyses were performed with the Student's t test (n=20). **F**, Representative images and statistical chart of mIHC staining of pancreatic cancer samples. TMAs of 140 pancreatic cancer were stained. Intact tissues were included in follow-up analysis. Samples were divided into two groups according to h-score of Pan-Kla. Proportion of each cell type in total cells was calculated. Statistical analyses were performed with Student's t test (n=140). Scale bar=0.1cm. **G**, Pan-Kla expression and 2-NBDG uptake tested using flow cytometry by each cell types in human paired tumors and peripheral blood. **H, I,** Gene ontology enrichment analysis of macrophages (**H**) and CD8+ T cells (**I**).

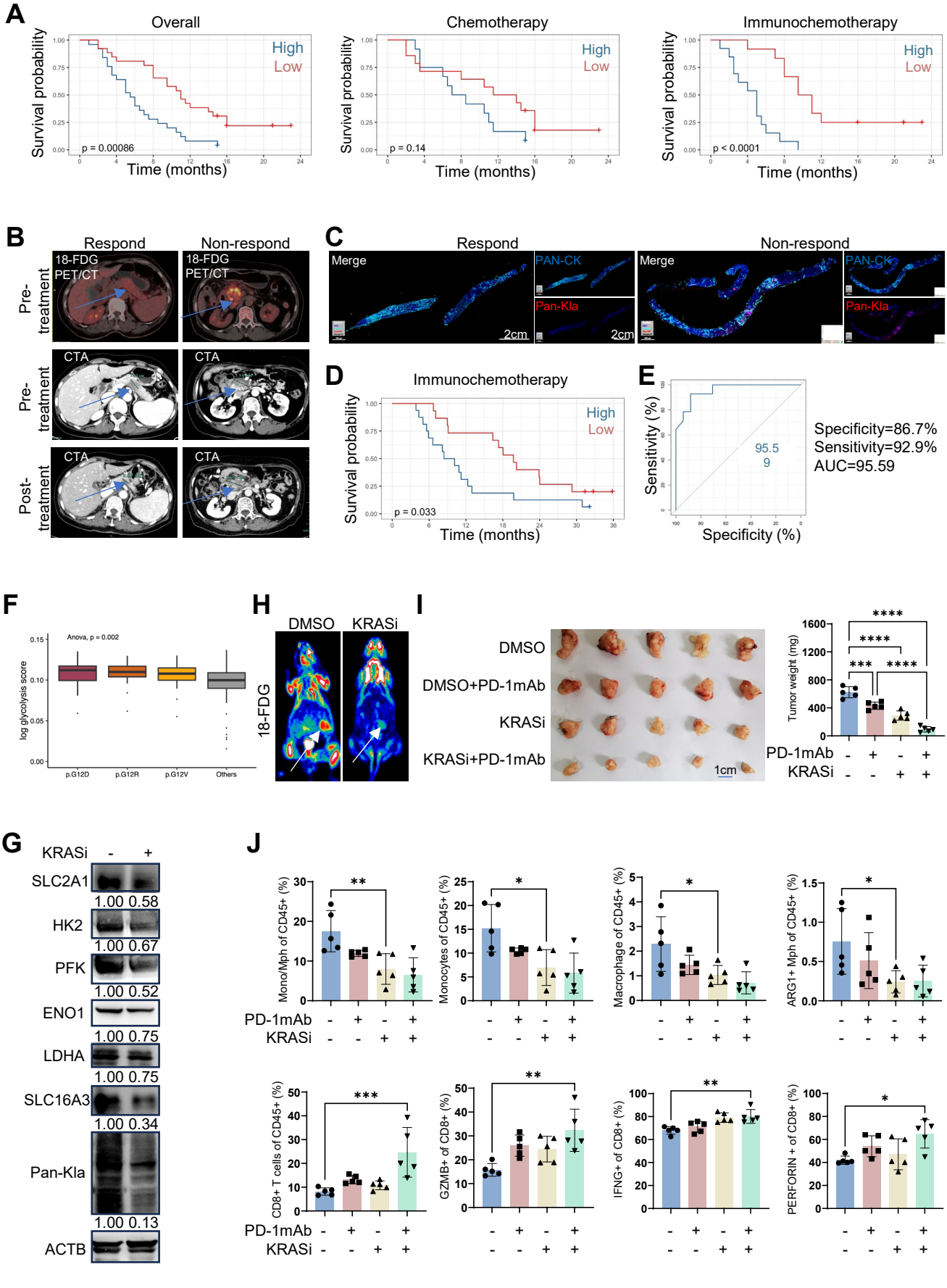
A
Overall
Chemotherapy
Immunochemotherapy
Survival probability
High
Low
p = 0.00086
p = 0.14
p < 0.0001
Time (months)
B
Respond
Non-respond
Pre-treatment
Post-treatment
18-FDG PET/CT
CTA
C
Respond
Non-respond
Merge
PAN-CK
Pan-Kla
2cm
D
Immunochemotherapy
p = 0.033
E
Sensitivity (%)
Specificity (%)
95.5
9
Specificity=86.7%
Sensitivity=92.9%
AUC=95.59
F
Anova, p = 0.002
log glycolysis score
p.G12D
p.G12R
p.G12V
Others
H
DMSO
KRASi
18-FDG
I
DMSO
DMSO+PD-1mAb
KRASi
KRASi+PD-1mAb
1cm
Tumor weight (mg)
PD-1mAb
KRASi
G
KRASi
SLC2A1
1.00 0.58
HK2
1.00 0.67
PFK
1.00 0.52
ENO1
1.00 0.75
LDHA
1.00 0.75
SLC16A3
1.00 0.34
Pan-Kla
1.00 0.13
ACTB
J
Mono/Mph of CD45+ (%)
Monocytes of CD45+ (%)
Macrophage of CD45+ (%)
ARG1+ Mph of CD45+ (%)
CD8+ T cells of CD45+ (%)
GZMB+ of CD8+ (%)
IFNG+ of CD8+ (%)
PERFORIN + of CD8+ (%)
PD-1mAb
KRASi

Figure 2. Elevated lactylation is associated with immunotherapy resistance in PDAC. A, Kaplan-Meier survival curves of progression-free survival for patients with PDAC based on the impact of ^{18}F-FDG uptake with treatment. The median of ^{18}F-FDG SUVmax was used to divide the cohort (cut off: 8.1). Statistical analyses were performed with Log-rank. **B**, Representative images of ^{18}F-FDG PET/CT and computed tomography angiography (CTA) of patients. Tumors were shown with a blue arrow. **C**, Pan-Kla levels were analyzed by immunostaining of 31 biopsy specimens. Representative images of patients were shown. Scale bar = 2cm. **D**, Overall survival analysis was performed based on mean fluorescence intensity of Pan-Kla immunostaining. **E**, ROC-AUC plot analysis was performed based on mean fluorescence intensity of Pan-Kla. Statistical analyses were performed with Log-rank. Prediction model of immunochemotherapy response situation was established. **F**, Glycolysis score of patients with different KRAS mutation status using TCGA-PAAD database. Statistical analyses were performed with One-way Anova. **G**, Protein expression analysis of KPC cells treated with MRTX1133 (1μM, 24h) or DMSO. **H**, Representative images of 18-FDG PET-CT of KPC orthotopic transplantation model treated with MRTX1133 (0.2 mg/mouse, i.p., qd) or DMSO. Tumors were shown with a white arrow. **I,** Orthotopic transplantation tumors and statistical analysis were shown. KPC mice were individually treated by anti-PD1mAb (100 μg/mouse, i.p., tid) or MRTX1133 (0.2 mg/mouse, i.p., qd). Statistical analyses were performed with One-way Anova (n=5). **J**, Proportions of each type of immunocytes and function markers in $CD8^+$ T cells. The immune microenvironment of orthotopic transplantation model with different treatments were compared. Statistical analyses were performed with One-way Anova (n=5).

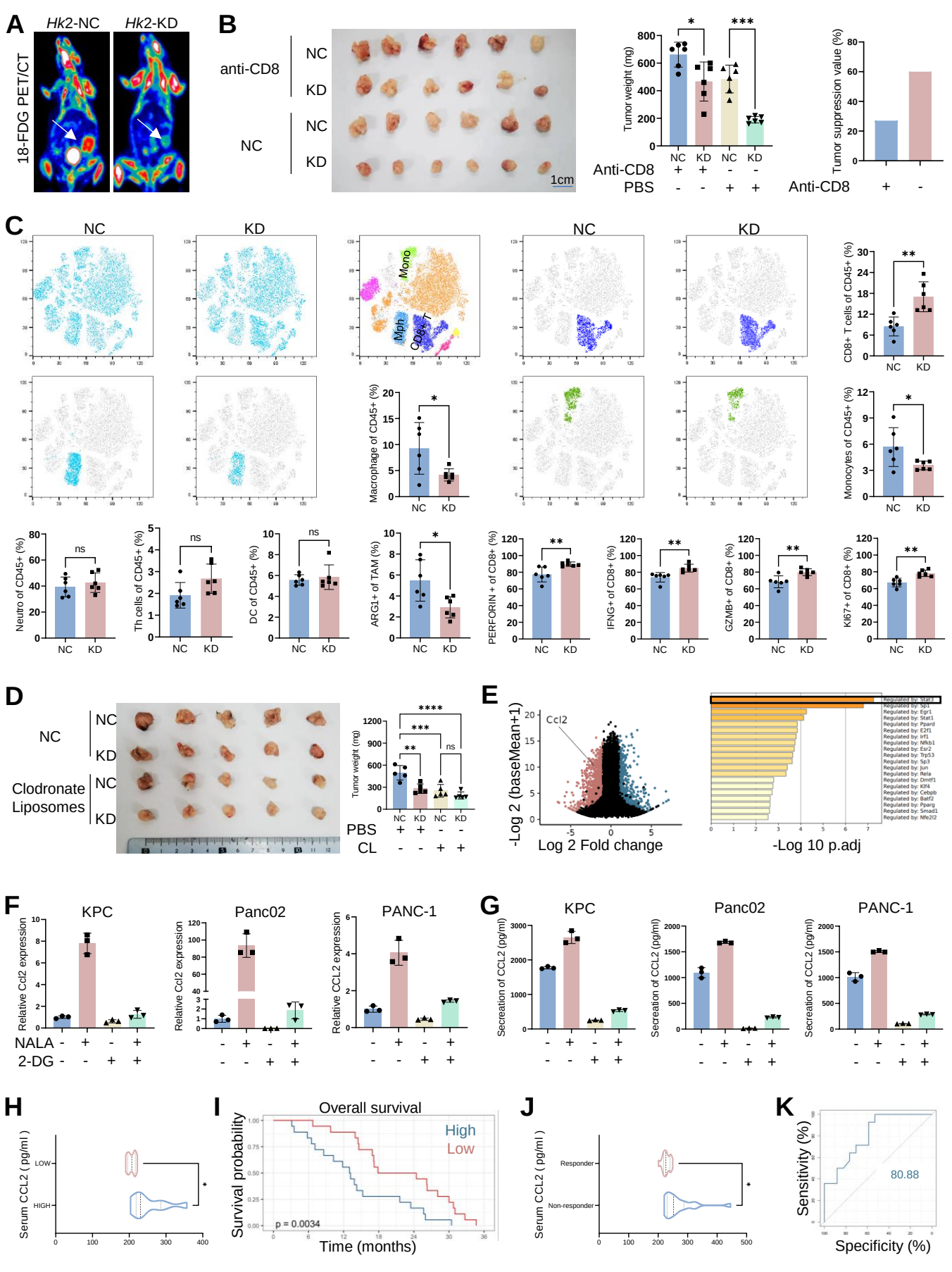
A
Hk2-NC
Hk2-KD
18-FDG PET/CT
B
anti-CD8
NC
KD
NC
KD
1cm
Tumor weight (mg)
Anti-CD8
PBS
Tumor suppression value (%)
C
NC
KD
Mono
Mph
CD8+ T
CD8+ T cells of CD45+ (%)
Macrophage of CD45+ (%)
Monocytes of CD45+ (%)
Neutro of CD45+ (%)
Th cells of CD45+ (%)
DC of CD45+ (%)
ARG1+ of TAM (%)
PERFORIN + of CD8+ (%)
IFNG+ of CD8+ (%)
GZMB+ of CD8+ (%)
Ki67+ of CD8+ (%)
D
Clodronate Liposomes
Tumor weight (mg)
PBS
CL
E
Ccl2
-Log 2 (baseMean+1)
Log 2 Fold change
-Log 10 p.adj
F
KPC
Panc02
PANC-1
Relative Ccl2 expression
Relative CCL2 expression
NALA
2-DG
G
Secreation of CCL2 (pg/ml)
H
Serum CCL2 (pg/ml)
LOW
HIGH
I
Overall survival
Survival probability
High
Low
p = 0.0034
Time (months)
J
Responder
Non-responder
K
Sensitivity (%)
Specificity (%)
80.88

Figure 3. Inhibiting glycolysis reduces the levels of CCL2 secreted by tumor. A, Representative images of 18-FDG PET-CT of *Hk2*-NC and *Hk2*-KD KPC orthotopic transplantation models. Tumors were shown with a white arrow. **B**, *Hk2*-NC and *Hk2*-KD KPC orthotopic transplantation mice were individually treated with or without anti-CD8 mAb (100 μg/mouse, i.p., tid). Statistical analyses were conducted with One-way Anova (n=6). **C**, t-SNE analysis and proportions of each type of immunocytes. Statistical analyses were performed with the Student's t test (n=6). **D**, Hk2-NC and Hk2-KD KPC orthotopic transplantation mice were individually treated with or without clodronate liposomes (1mg/mouse, i.p, q7d). Statistical analyses were performed with One-way Anova (n=5). **E**, Volcano map of the RNAseq and transcriptional activity assay. KPC cells were treated with 2-DG (HK2 inhibitor, 10mM, 24h), and differentially expressed genes were shown. Ccl2 was significantly downregulated when treated with 2-DG. Top 1,000 downregulated genes were validated by transcriptional activity assay using metascape. **F**, Relative *Ccl2* mRNA expression was shown **G**, Relative CCL2 secretion tested by ELISA was shown. **H**, Concentration of serum CCL2. A total of 20 fresh PDAC samples were divided into two groups according to Pan-Kla expression. Statistical analyses were performed with the Students' t test (n=20). **I,** Overall survival analysis was performed based on concentration of serum CCL2. Patients were divided into two groups according to the medium amount of serum CCL2. Statistical analyses were performed with Log-rank (n=36). **J**, Concentration of serum CCL2 tested by ELISA. 31 PDAC samples involved in the CISPD3 RCT study were divided into two groups according to their response to immunochemotherapy. **K**, ROC-AUC plot analysis was performed based on the concentration of CCL2. Prediction model of immunochemotherapy response situation was established.

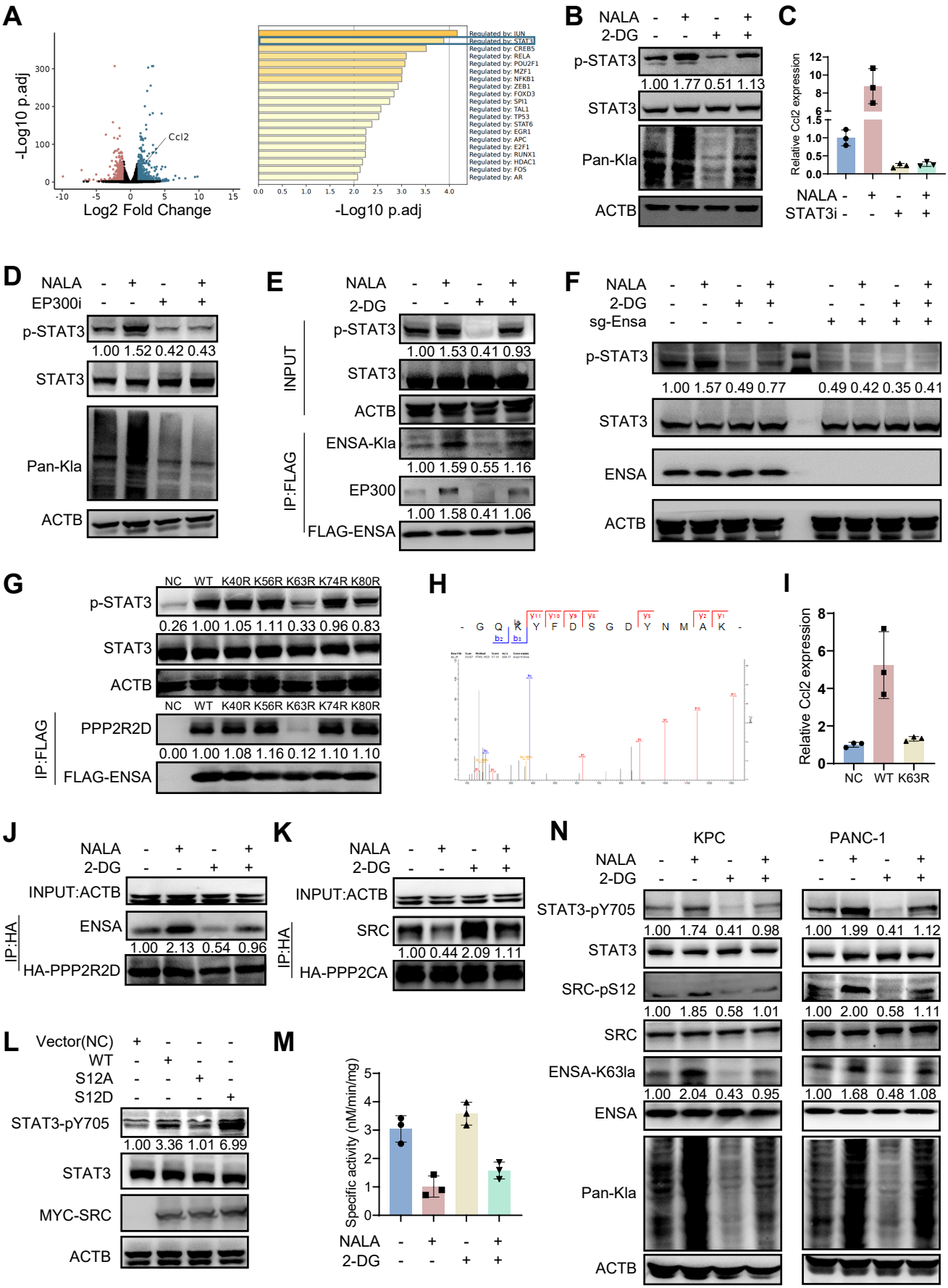
A
-Log10 p.adj
Log2 Fold Change
Ccl2
Regulated by: JUN
Regulated by: STAT3
Regulated by: CREB5
Regulated by: RELA
Regulated by: POU2F1
Regulated by: MZF1
Regulated by: NFKB1
Regulated by: ZEB1
Regulated by: FOXD3
Regulated by: SPI1
Regulated by: TAL1
Regulated by: TP53
Regulated by: STAT6
Regulated by: EGR1
Regulated by: APC
Regulated by: EZF1
Regulated by: RUNX1
Regulated by: HDAC1
Regulated by: FOS
Regulated by: AR
-Log10 p.adj
B
NALA
2-DG
p-STAT3
1.00 1.77 0.51 1.13
STAT3
Pan-Kla
ACTB
C
Relative Ccl2 expression
NALA
STAT3i
D
NALA
EP300i
p-STAT3
1.00 1.52 0.42 0.43
STAT3
Pan-Kla
ACTB
E
NALA
2-DG
INPUT
p-STAT3
1.00 1.53 0.41 0.93
STAT3
ACTB
IP:FLAG
ENSA-Kla
1.00 1.59 0.55 1.16
EP300
1.00 1.58 0.41 1.06
FLAG-ENSA
F
NALA
2-DG
sg-Ensa
p-STAT3
1.00 1.57 0.49 0.77
0.49 0.42 0.35 0.41
STAT3
ENSA
ACTB
G
NC WT K40R K56R K63R K74R K80R
p-STAT3
0.26 1.00 1.05 1.11 0.33 0.96 0.83
STAT3
ACTB
NC WT K40R K56R K63R K74R K80R
IP:FLAG
PPP2R2D
0.00 1.00 1.08 1.16 0.12 1.10 1.10
FLAG-ENSA
H
- G Q K Y F D S G D Y N M A K -
I
Relative Ccl2 expression
NC WT K63R
J
NALA
2-DG
INPUT:ACTB
IP:HA
ENSA
1.00 2.13 0.54 0.96
HA-PPP2R2D
K
NALA
2-DG
INPUT:ACTB
IP:HA
SRC
1.00 0.44 2.09 1.11
HA-PPP2CA
N
KPC
PANC-1
NALA
2-DG
STAT3-pY705
1.00 1.74 0.41 0.98
1.00 1.99 0.41 1.12
STAT3
SRC-pS12
1.00 1.85 0.58 1.01
1.00 2.00 0.58 1.11
SRC
ENSA-K63la
1.00 2.04 0.43 0.95
1.00 1.68 0.48 1.08
ENSA
Pan-Kla
ACTB
L
Vector(NC)
WT
S12A
S12D
STAT3-pY705
1.00 3.36 1.01 6.99
STAT3
MYC-SRC
ACTB
M
Specific activity (nM/min/mg)
NALA
2-DG

Figure 4. ENSA K63 lactylation upregulates STAT3-CCL2 signaling via PP2A and SRC. A, Volcano map of the RNA-seq analysis. Top 1,000 upregulated genes were deconvoluted to reveal related transcriptional factors using metascape. **B**, Protein expression analysis of KPC cells treated with 2-DG (10mM, 24h) or NALA (40mM, 24h). **C**, Relative *Ccl2* mRNA expression was shown with three technical replicates. KPC cells were treated with STAT3-IN-11 (1μM, 24h) or NALA (40mM, 24h). **D**, Protein expression analysis of KPC cells treated with A-485 (EP300 inhibitor, 1μM, 24h) or NALA (40mM, 24h). **E**, Protein expression and immunoprecipitation-immunoblotting analyses of KPC cells treated with 2-DG (10mM, 24h) or NALA (40mM, 24h). Anti-FLAG antibody was used to immunoprecipitate ENSA-FLAG proteins. **F**, Protein expression analysis of *Ensa*-NC and *Ensa*-KO KPC cells treated with 2-DG (10mM, 24h) or NALA (40mM, 24h). **G**, Protein expression analysis of each *Ensa*-KO KPC cell line overexpressing ENSA-NC, ENSA-WT-FLAG, ENSA-K40R-FLAG, ENSA-K56R-FLAG, ENSA-K63R-FLAG, ENSA-K74R-FLAG or ENSA-K80R-FLAG. **H**, Mass spectrum analysis revealed that ENSA is lactylated at K63 site. **I,** Relative *Ccl2* mRNA expression of each *Ensa*-KO KPC cell line overexpressing vector control, ENSA-WT or ENSA-K63R was shown. **J**, Protein expression and immunoprecipitation-immunoblotting analyses of KPC-HA-PPP2R2D cell line treated with 2-DG (10mM, 24h) or NALA (40mM, 24h). Anti-HA antibody was used to immunoprecipitate HA-PPP2R2D proteins. **K**, Protein expression and immunoprecipitation-immunoblotting analysis of KPC-HA-PPP2CA cell line treated with 2-DG (10mM, 24h) or NALA (40mM, 24h). Anti-HA antibody was used to immunoprecipitate HA-PPP2CA proteins. **L**, Protein expression analysis of each KPC cell line overexpressing vector (control), SRC-WT, SRC-S12A or SRC-S12D. **M**, SRC-pS12-specific activity of PP2A phosphatase. SRC-pS12 cell-penetrating peptide (HLYVSPWGG-SKPKDApSQRRRSL) was incubated with KPC cells treated with 2-DG (10mM, 24h) or NALA (40mM, 24h). **N**, Protein expression analysis of KPC and PANC-1 cells treated with 2-DG (10mM, 24h) or NALA (40mM, 24h).

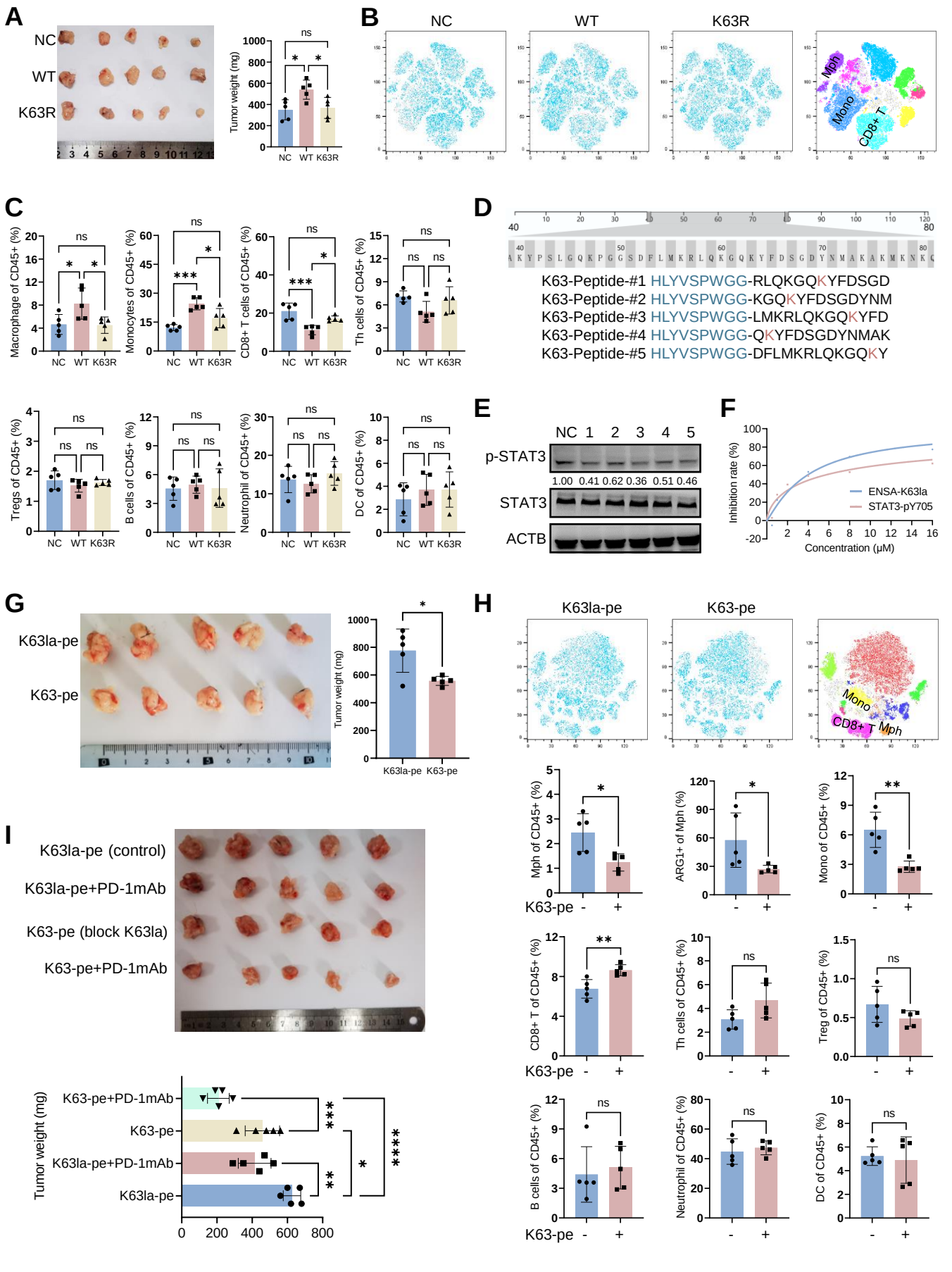
A
NC
WT
K63R
Tumor weight (mg)
ns
B
NC
WT
K63R
Mph
Mono
CD8+ T
C
Macrophage of CD45+ (%)
Monocytes of CD45+ (%)
CD8+ T cells of CD45+ (%)
Th cells of CD45+ (%)
Tregs of CD45+ (%)
B cells of CD45+ (%)
Neutrophil of CD45+ (%)
DC of CD45+ (%)
D
K63-Peptide-#1 HLYVSPWGG-RLQKGQKYFDSGD
K63-Peptide-#2 HLYVSPWGG-KGQKYFDSGDYNM
K63-Peptide-#3 HLYVSPWGG-LMKRLQKGQKYFD
K63-Peptide-#4 HLYVSPWGG-QKYFDSGDYNMAK
K63-Peptide-#5 HLYVSPWGG-DFLMKRLQKGQKY
E
NC 1 2 3 4 5
p-STAT3
1.00 0.41 0.62 0.36 0.51 0.46
STAT3
ACTB
F
Inhibition rate (%)
Concentration (μM)
ENSA-K63la
STAT3-pY705
G
K63la-pe
K63-pe
Tumor weight (mg)
H
K63la-pe
K63-pe
Mono
CD8+ T
Mph
Mph of CD45+ (%)
ARG1+ of Mph (%)
Mono of CD45+ (%)
CD8+ T of CD45+ (%)
Th cells of CD45+ (%)
Treg of CD45+ (%)
B cells of CD45+ (%)
Neutrophil of CD45+ (%)
DC of CD45+ (%)
I
K63la-pe (control)
K63la-pe+PD-1mAb
K63-pe (block K63la)
K63-pe+PD-1mAb
Tumor weight (mg)

Figure 5. Design of a peptide inhibitor specifically targeting ENSA-K63la. A, *Ensa*-KO KPC cells stably expressing vector control, ENSA-WT and ENSA-K63R were orthotopically transplanted into mice and tumor growth was analyzed. Statistical analyses were performed with One-way Anova (n=5). **B, C**, t-SNE analysis (**B**) and proportions (**C**) of each type of immunocytes in the tumors in (**A**). The immune profiling was analyzed using Cytek. Statistical analyses were performed with One-way Anova (n=5). **D,** Human and mouse ENSA protein sequences were shown. Cell-penetrating peptide targeting ENSA-K63la was designed around K63 site. **E**, Protein expression analysis of KPC cells treated with individual K63-peptide (10μM, 24h). **F**, Relative inhibition rate of STAT3 Y705 phosphorylation. KPC cells treated with K63-peptide inhibitor 3 (HLYVSPWGG-LMKRLQKGQKYFD) and K63la-peptide control 3 (HLYVSPWGG-LMKRLQKGQKlaYFD) with different concentrations (0μM; 0.5μM; 1μM; 2μM; 4μM; 8μM; 16μM) for 24 hours. Immunoblotting band intensity was measured using Image J. The relative levels of ENSA-K63la and STAT3-pY705 was normalized by the level of ACTB. The relative inhibition rate at a certain concentration was calculated by 1- expression (K63 inhibitor 3)/expression (K63la control 3). IC50 was calculated by nonlinear regression. **G**, Orthotopic transplantation tumors and statistical analysis were shown. KPC orthotopic transplantation mice were treated with K63la-pe control 3 (control) or K63-pe inhibitor 3 (0.2 mg/mouse, i.p., qd). Tumor growth was analyzed with the Student's t test (n=5). **H**, t-SNE analysis and proportions of each type of immunocytes in the tumors in (**G**). The immune profile of tumors was analyzed using Cytek. Statistical analyses were performed with the Student's t test (n=5). **I,** Orthotopic transplantation tumorsand statistical analysis were shown. KPC mice were treated with anti-PD1 mAb (100 μg/mouse, i.p., tid), K63la-pe control 3 or K63-pe inhibitor 3 (0.2 mg/mouse, i.p., qd). Tumor growth was analyzed with One-way Anova (n=5).

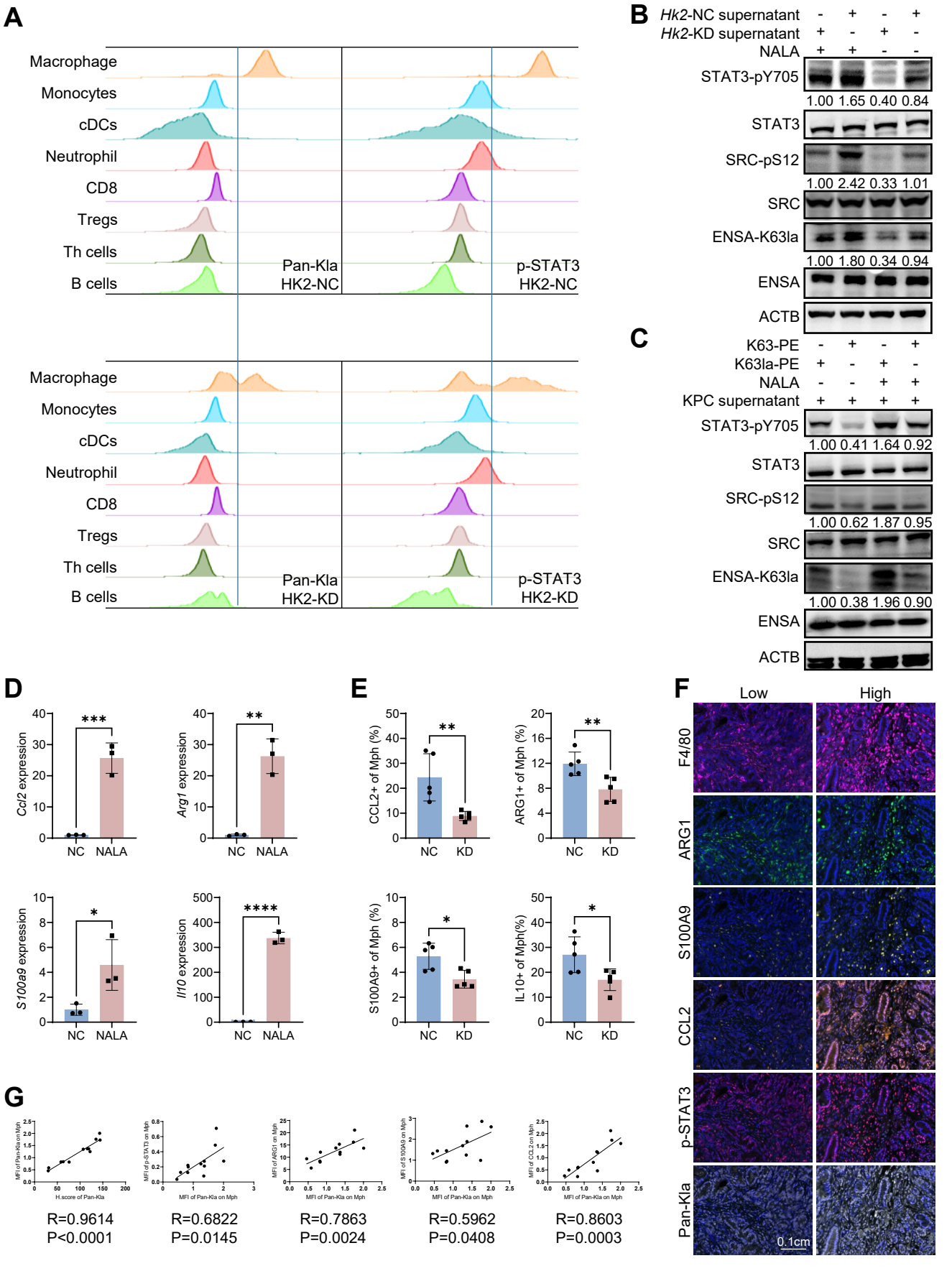
A
Macrophage
Monocytes
cDCs
Neutrophil
CD8
Tregs
Th cells
B cells
Pan-Kla
HK2-NC
p-STAT3
HK2-NC
Pan-Kla
HK2-KD
p-STAT3
HK2-KD
B
Hk2-NC supernatant - + - +
Hk2-KD supernatant + - + -
NALA + + - -
STAT3-pY705
1.00 1.65 0.40 0.84
STAT3
SRC-pS12
1.00 2.42 0.33 1.01
SRC
ENSA-K63la
1.00 1.80 0.34 0.94
ENSA
ACTB
C
K63-PE - + - +
K63la-PE + - + -
NALA - - + +
KPC supernatant + + + +
STAT3-pY705
1.00 0.41 1.64 0.92
STAT3
SRC-pS12
1.00 0.62 1.87 0.95
SRC
ENSA-K63la
1.00 0.38 1.96 0.90
ENSA
ACTB
D
Ccl2 expression
Arg1 expression
S100a9 expression
Il10 expression
NC
NALA
E
CCL2+ of Mph (%)
ARG1+ of Mph (%)
S100A9+ of Mph (%)
IL10+ of Mph(%)
NC
KD
F
Low
High
F4/80
ARG1
S100A9
CCL2
p-STAT3
Pan-Kla
0.1cm
G
R=0.9614
P<0.0001
R=0.6822
P=0.0145
R=0.7863
P=0.0024
R=0.5962
P=0.0408
R=0.8603
P=0.0003

Figure 6. Lactate accumulation reprograms TAMs by ENSA lactylation. A, Pan-Kla and p-STAT3 expression were tested using intracellular flow cytometry in each cell types from *Hk2*-NC and *Hk2*-KD KPC orthotopic tumors. **B**, Protein expression analysis of BMDM pretreated with *Hk2*-NC and *Hk2*-KD KPC cell supernatant and then treated with NALA (10mM, 24h). **C**, Protein expression analysis of BMDM pretreated with KPC cell supernatant (1:1, 24h) and then treated with K63la-pe control 3 or K63-pe inhibitor 3 (10μM, 24h). **D**, BMDM was pretreated with KPC supernatant (1:1, 24h) and then treated with NALA (40mM, 24h). Relative *Ccl2, Arg1, S100A9* and *Il10* mRNA expression levels were shown. **E**, CCL2, IL10, ARG1, S100A9 expression in TAMs. Flow cytometry was used. Statistical analyses were performed with the Students' t test (n=5). **F**, Representative images of multiplex immunohistochemistry staining of KTC tumor samples from transgenic mice (LSL-Kras (G12D/+); Tgfbr2 (flox/flox); p48 (Cre/+)). Representative images of paraffin sections with high or low Pan-Kla expression were shown. **G**, Simple linear regression was used to reveal correlation of pSTAT3, CCL2, ARG1, S100A9 and Pan-Kla (n=12).

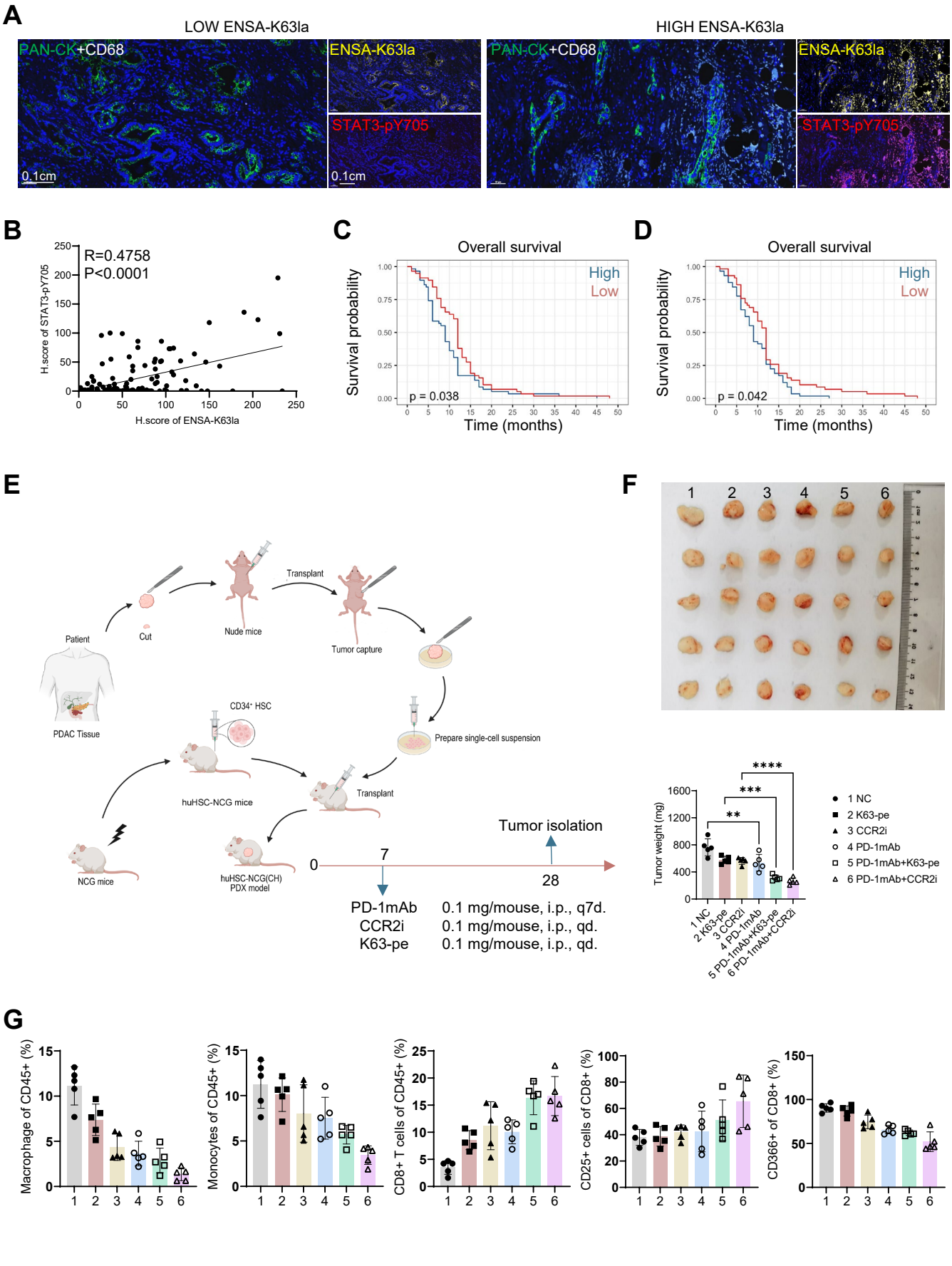
A
LOW ENSA-K63la
HIGH ENSA-K63la
PAN-CK+CD68
ENSA-K63la
STAT3-pY705
0.1cm
B
R=0.4758
P<0.0001
H.score of STAT3-pY705
H.score of ENSA-K63la
C
Overall survival
Survival probability
High
Low
p = 0.038
Time (months)
D
Overall survival
Survival probability
High
Low
p = 0.042
Time (months)
E
Patient
Cut
Nude mice
Transplant
Tumor capture
PDAC Tissue
CD34+ HSC
Prepare single-cell suspension
huHSC-NCG mice
Transplant
NCG mice
huHSC-NCG(CH)
PDX model
Tumor isolation
0
7
28
PD-1mAb 0.1 mg/mouse, i.p., q7d.
CCR2i 0.1 mg/mouse, i.p., qd.
K63-pe 0.1 mg/mouse, i.p., qd.
F
1 2 3 4 5 6
Tumor weight (mg)
1 NC
2 K63-pe
3 CCR2i
4 PD-1mAb
5 PD-1mAb+K63-pe
6 PD-1mAb+CCR2i
G
Macrophage of CD45+ (%)
Monocytes of CD45+ (%)
CD8+ T cells of CD45+ (%)
CD25+ cells of CD8+ (%)
CD366+ of CD8+ (%)

Figure 7. ENSA-K63la/STAT3-pY705/CCL2 axis is a therapeutic target for human PDAC. A, Representative images of multiplex immunohistochemistry of human PDAC tumor tissues. **B**, Simple linear regression was used to reveal correlation of ENSA-K63la and STAT3-pY705. Intact tissues with survival data were included in follow-up analysis (n=116). **C**, Overall survival analysis was performed based on max fluorescence intensity of ENSA-K63la. Statistical analyses were performed with Log-rank (n=116). **D**, Overall survival analysis was performed based on mean fluorescence intensity of STAT3-pY705. Statistical analyses were performed with Log-rank (n=116). **E**, Schematic diagram for generating humanized PDAC models. **F**, Subcutaneous transplantation tumors and statistical analysis were shown. Statistical analyses were performed with One-way Anova (n=5). **G**, Proportions of each cell type of immunocytes and each function marker in CD8+ T cells.